WIICT2019

Proceedings of the Workshop on Innovation on Information and Communication Technologies 2019

Institute ITACA
Information and Communication Technologies

Editors:
Dr. Carlos Fernandez-Llatas
Dra. Maria Guillen

Committees

Organizing Committee

- **Chair**:Maria Guillem, Universitat Politècnica de València, Spain
- Alberto Bonastre, Universitat Politècnica de València, Spain
- Jose Manuel Catala, Universitat Politècnica de València, Spain
- Montserrat Robles, Universitat Politècnica de València, Spain
- Carlos Fernández-Llatas, Universitat Politècnica de València, Spain
- Jose Mariano Dahoui, Universitat Politècnica de València, Spain
- Isidora Navarro, Universitat Politècnica de València, Spain
- Manuel Traver Salcedo, Universitat Politècnica de València, Spain
- Lucia Aparici, Universitat Politècnica de València, Spain

Scientific Committee

- **Chair**: Carlos Fernandez-Llatas, Universitat Politècnica de València, Spain
- Paulo de Carvalho, University of Coimbra, Portugal
- Anna-Maria Bianchi, Politecnico di Milano, Italy
- Jorge Munoz-Gama, Pontificia Universidad Catolica de Chile
- Fernando Seoane, Karolinska Institutet
- Jorge Henriques, University of Coimbra, Portugal
- Cenk Demiroglu, Ozyegin University, Turkey
- Johan Gustav Bellika, National Center of Telemedicine, Norway
- Yigzaw Kassaye Yitbarek, University of Tromso, Norway
- Raymundo Barrales, Universidad Autónoma Metropolitana de México
- Frank Y. Li, University of Agder, Norway
- Pilar Sala, MySphera., Spain
- Alvaro Martinez, MySphera, Spain
- Jose Carlos Campelo, Universitat Politècnica de València, Spain
- Juan Vicente Capella, Universitat Politècnica de València, Spain
- Antonio Mocholí, Universitat Politècnica de València, Spain
- Sara Blanc, Universitat Politècnica de València, Spain
- Juan-Carlos Baraza-Calvo, Universitat Politècnica de València, Spain
- Juan Carlos Ruiz, Universitat Politècnica de València, Spain
- Joaquin Gracia, Universitat Politècnica de València, Spain
- David De Andres, Universitat Politècnica de València, Spain
- Ricardo Mercado, Universitat Politècnica de València, Spain
- Miguel Rodrigo Bort, Universitat Politècnica de València, Spain
- Alejandro Liberos, Universitat Politècnica de València, Spain
- Jorge Pedrón, Universitat Politècnica de València, Spain
- Lenin Lemus, Universitat Politècnica de València, Spain
- Vicente Traver, Universitat Politècnica de València, Spain
- Antonio Martinez-Millana, Universitat Politècnica de València, Spain
- Jose Luis Bayo-Monton, Universitat Politècnica de València, Spain
- Lucia Aparici-Tortajada, Universitat Politècnica de València, Spain
- Juan Miguel García-Gomez, Universitat Politècnica de València, Spain
- Elies Fuster, Universitat Politècnica de València, Spain
- Carlos Saez, Universitat Politècnica de València, Spain
- Miguel Angel Rodriguez-Hernandez, Universitat Politècnica de València, Spain
- Canek Portillo Jimenez, Universitat Politècnica de València, Spain
- Ángel Perles, Universitat Politècnica de València, Spain
- Julian Camilo Romero-Chavarro, Universitat Politècnica de València, Spain
- Diego Boscá Tomás, Universitat Politècnica de València, Spain
- Luis Tello-Oquendo, Universitat Politècnica de València, Spain

- Israel Leyva-Mayorga, Universitat Politècnica de València, Spain
- Ángel Sanchis-Cano, Universitat Politècnica de València, Spain
- Luis José Saiz Adalid, Universitat Politècnica de València, Spain
- Gema Ibañez, Universitat Politècnica de València, Spain
- Pedro Yuste, Universitat Politècnica de València, Spain
- Daniel Gil Tomàs, Universitat Politècnica de València, Spain
- Conrado Javier Calvo Saiz, Universitat Politècnica de València, Spain
- Sabina Asensio, Universitat Politècnica de València, Spain
- Beatriz Garcia-Baños, Universitat Politècnica de València, Spain
- Diogo Nunes, University of Coimbra, Portugal
- Adriana Leal, University of Coimbra, Portugal
- Zoe Valero Ramón, Universitat Politècnica de València, Spain

Table of Contents

Development of mobile application for the management of parking in real time through the use of magnetic loops

Ferran Mocholí Belenguer[1], César Aroca García[1], and Antonio Mocholí Salcedo[1]

[1] Instituto ITACA, Universitat Politècnica de València, Camino de vera s/n
46022 Valencia, Spain

fermocbe@upv.es
ceargar@teleco.upv.es
amocholi@eln.upv.es

Abstract. When trying to respond to basic questions such as the number and type of vehicles that circulate on the road, the speed at which they circulate or the direction in which they do it, there are a lot of technologies related to Intelligent Transportation Systems (ITS) that can be used. However, despite the fact that infrastructure have changed significantly in recent years due to the continuous evolution of the technology, magnetic loops continue to be the reference traffic sensor because of their simplicity and operating mode. Therefore, with the aim of adding even more functionalities to this reference sensor, this paper presents the design of a system together with a mobile application for parking management in real time through the use of magnetic loops, which will be able to detect free parking spaces on public roads and manage them through a database so that users can consult said information through their smartphones.

1 Introduction

Currently, the sale and registration of vehicles continues increasing both in Spain and in the rest of the world, being the displacement by private vehicles the most common method of transport within the main cities [1]. Therefore, the main agencies responsible for traffic management are trying to establish new environmental and ecological policies in order to encourage the use of public transport and reduce the number of vehicles on the roads. However, the annual average of time lost in traffic jams in Spain is 17 hours per year, a figure that normally increases in relation to the size of the city: 26 annual hours in Valencia, 28 annual hours in Barcelona and 42 annuals hours in Madrid [2], which translate every year into economic losses and health problems derived from substances expelled by the combustion engines of vehicles.

In addition, it is estimated that about 30% of average traffic corresponds to the search for parking, losing 1.35€ on average for each unnecessary search and expelling 1.3 kg of CO_2 in the atmosphere [3]. In fact, according to studies by the Dirección General de Tráfico (DGT), when there are no cars, NO_2 levels are reduced by 40%.

C.Fernandez-Llatas and M.Guillen (Ed.):
Workshop on Innovation on
Information and Communication Technologies
(ITACA-WIICT 2019)

ISBN 978-84-09-17526-0

Then, if these values are extrapolated to cities such as Madrid where traffic congestion accounts for 19% of total peak traffic, NO_2 emissions due to traffic would be reduced by 7.6% and the emissions due to the parking search by 2.3%. It is true that the environmental problem would be slightly reduced if the mobile fleet were upgraded to an electric one, but other problems such as the economic loss due to the time spent in a traffic jam or traffic inefficiency would still exist.

Currently there are no systems implemented in the cities that inform in real time about the availability of free parking spaces on public roads. However, there are several similar solutions in private car parks through the use of laser and ultrasound sensors. Then, with the implementation of this system and its corresponding mobile application, this service would be available to any citizen. In addition, infrastructure that is widely known and already in operation would be reused, which would facilitate its implementation.

The increase in Internet of Things (IoT) devices is expected to be greater once 5G communication technologies are implemented, which will have higher speeds than the current ones and a very low latency, which will cause, among other benefits, that this type of devices proliferate. Therefore, it seems logical to design an application that is capable of detecting free parking spaces by means of classic road sensors such as magnetic loops, which would thus become elements of IoT. This would reduce traffic congestion and improve the quality of life of citizens. Moreover, it is known that the management and control of traffic is one of the greatest current concerns both socially and politically.

2 Intelligent Transportation Systems

Intelligent Transportation Systems (ITS) are the set of tools and services that, through the innovations of information and communication technologies, are used to manage the mobility of people and the transport of goods. These ITS can be both terrestrial, including their application in roads and railways, as well as maritime or air, and their main purpose is that users are better informed and make a safer, more coordinated and intelligent use of transport networks.

However, it was the inclusion of telecommunications and ICT in the sector which caused a major revolution in it, since it had traditionally been reserved for the branch of Civil Engineering. This use of ICT together with ITS significantly improved the environmental impact and the efficiency, safety and protection of road transport, guaranteeing levels of competitiveness far superior to the previous ones.

The number of vehicles worldwide has increased progressively in recent years despite the slight stagnation caused by the economic crisis of 2008. In 2016, there were more than 32 million vehicles in Spain, an amount that is expected to exceed 33 million in the next years [1]. However, this increase in vehicles requires the implementation of systems to more efficiently manage mobility and traffic management.

The first traffic management system was created in 1925 by Charles Adler, who was an american engineer and inventor. This system was called "automatic speed control system" and was composed of a series of magnets buried under the road located 20 meters from dangerous points, so that when drivers exceeded 24 km / h, it activated a series of relays installed in the car that turned off the engine. Once the vehicle passed through other similar magnets, the engine was automatically started again. In addition, Adler also worked on the development of the first traffic light in the United States, serving as the basis for the current traffic lights.

However, currently the information is not treated individually. Today there is a global system composed of three large subsystems that are organized as shown in Figure 1. This system consists of:

- Traffic Management Centers: are the units responsible for control tasks and supervision of traffic, as well as assistance and information to road users. All the generated data are centralized, which are treated using appropriate techniques and procedures to manage traffic in a more efficient way.

- Road equipment: sensors, detectors and actuators such as traffic lights, magnetic loops or laser and radar technology to capture all kinds of information about vehicles and the state of the roads.

- Communications network: set of technologies that connect the aforementioned equipment with the corresponding management centers.

Fig. 1. Organization of a Traffic Control System.

3 Magnetic Loops

Magnetic loops are the most common sensors on roads around the world since they are an affordable and highly developed technology with a simple operation that is not affected by environmental conditions [4]. Even though they might seem outdated, these are actually a widely extended and well-known reliable technology that offers good performance at a low price. Proof of this is that today they continue to be installed on the roads and they are even fundamental elements in the new algorithms for traffic management [5]. That is the reason why we decided to use this type of technology for our parking application.

Their operation is straightforward, since it is based on the impedance variation that is recorded in the magnetic loops during the passage of vehicles over them, and as shown in Figure 2, an entire system usually consists of three parts:

I. A magnetic loop formed by a wire with one or more turns superficially buried in the pavement.
II. A cable that links the magnetic loop with the control booth, which is also buried in the pavement.
III. An electronic unit located in the control booth that contains an oscillator and amplifiers to excite the inductive loop.

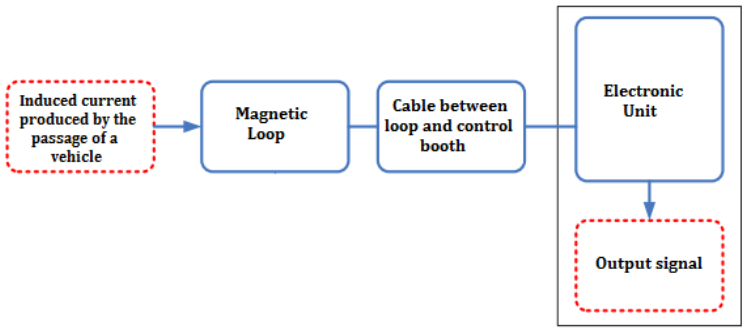

Fig. 2. Magnetic loop system scheme.

In order to have a better understanding of how they work, there are many publications and bibliography [6] since they are one of the most widespread sensors. However, a brief physical explanation is provided in the following points:

- The electronic unit together with the magnetic loop form an oscillator circuit.

- The current which passes through the loop produces a magnetic field $\vec{H}$ around the cable as shown in Equation 1, where N is the number of turns of the loop, I is the current expressed in Amperes and l is the length of the loop expressed in meters.

$$\vec{H} = \frac{N \cdot I}{l} \tag{1}$$

- This magnetic field $\vec{H}$ produces a magnetic flux $\emptyset$ through the loop as shown in Equation 2, where $\vec{B}$ is the magnetic flux density, $\vec{S}$ is the surface enclosed by the loop, μ_r is the relative magnetic permeability of the medium and μ_o is a constant value $(4\pi \cdot 10^{-7}$ N / A^2).

$$\emptyset = \vec{B} \cdot \vec{S} = \mu_r \cdot \mu_o \cdot \vec{H} \cdot \vec{S} \tag{2}$$

- The result is that the inductance of a common single loop L expressed in Henrys is obtained as:

$$L = \frac{N \cdot \emptyset}{I} = \frac{N \cdot \vec{B} \cdot \vec{S}}{I} \tag{3}$$

In this way, when a vehicle or any object built with ferromagnetic materials passes through the magnetic field generated by a magnetic loop buried on the road with a surface area $\vec{S}$, a number of turns N and a current intensity I as shown in Figure 3, there is a decrease in the global magnetic field because of the currents that are induced in the vehicle.

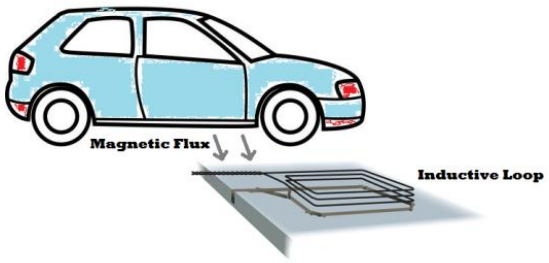

Fig. 3. Magnetic loop operation mode.

As seen in Equation 3, the loop inductance is proportional to the magnetic flux, which causes that when passing a vehicle over it, the inductance also decreases. Moreover, like any oscillator circuit, the oscillation frequency of the whole system will be given by:

$$f = \frac{k}{L} \tag{4}$$

Being k a constant that depends on the characteristics of the electronic components used in the construction of the oscillator circuit. Thus, when a vehicle passes over a loop, we can obtain what is commonly known as 'the vehicle magnetic profile' or 'the vehicle inductance signature' by analyzing the inductance or frequency variation recorded. This magnetic profile is different for each type of vehicle as seen in Figure 4, which allows to classify the different vehicles as motorcycles, cars, trucks and buses.

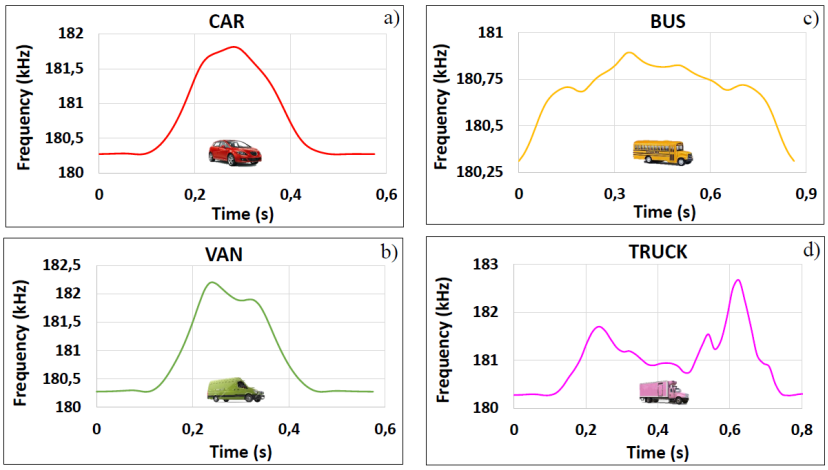

Fig. 4. Magnetic profiles from (a) car, (b) van, (c) bus and (d) truck.

However, this time our system will not need to classify vehicles or extract classic parameters such as their speed or length. Our system will simply have to detect changes in the frequency of oscillation for a certain time, which will mean that a car has parked in a parking space. For that purpose, magnetic loops would be installed in the parking spaces that were considered appropriate along with their electric units. An example of our system is shown in Figure 5.

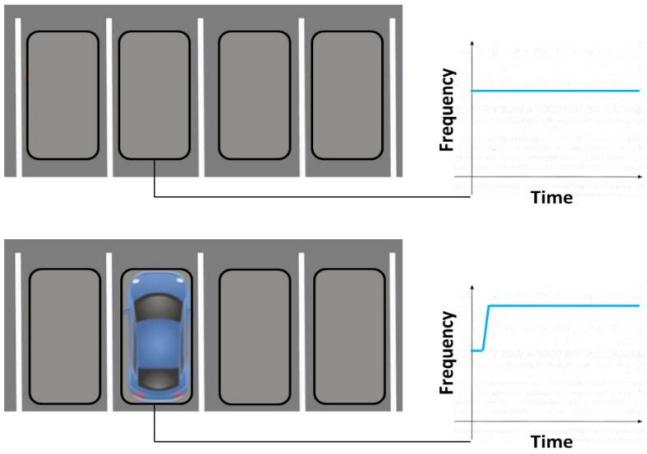

Fig. 5. Diagram of our parking system.

4 Parking management

The general objective of this work was to create a mobile application that detected free parking spaces through the use of magnetic loops and updated the information in real time. In order to achieve this goal, the following equipment shown in Figure 6 has been used:

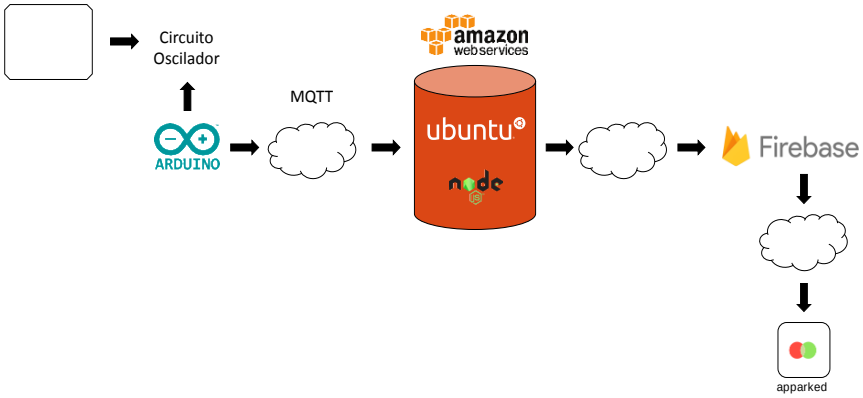

Fig. 6. Diagram of interconnection of the elements that intervene in the parking system.

- Arduino: is a small board computer, which is part of an open source and hardware project. For the development of this work, the Arduino UNO version has been used, which consists of 14 digital pins and 6 analog pins. It carries the ATmega328P processor with a clock speed of 16 MHz. In addition, an Ethernet Shield is also used to provide it with connectivity to internet.

- MQTT: stands for MQ Telemetry Transport. It is a publish, extremely simple and lightweight messaging protocol, designed for constrained devices and low-bandwidth, high-latency or unreliable networks. The design principles are to minimize network bandwidth and device resource requirements whilst also attempting to ensure reliability and some degree of assurance of delivery. One of its main objectives is to make the protocol ideal for the emerging world of the Internet of things, and that is the reason why MQTT was chosen to perform the exchange of messages between Arduino and the server.

- Amazon Web Services: belongs to the company Amazon Inc. and is responsible for providing cloud computing service. Among these services, there are servers, of which an E2C or Elastic Compute Cloud instance has been used. These instances allow any computer to run applications.

- Firebase: is a Google mobile application development platform which offers different services. However, Cloud Firestore has been finally used. It is a flexible, scalable and NoSql database that allows to update information in real time and store and synchronize data between the client and the database, all transparently to the user. It also offers assistance when the connection is lost by saving the data from the last time you had a connection.

- Apparked: an application called apparked has been finally developed in Swift 5 language, available for iOS devices through the Xcode SDK. Its mode of operation, which is tremendously intuitive, and its appearance are shown in Figure 7.

  This results in the mobile application shown in Figure 7, in which the user can see in real time the availability of parking spaces.

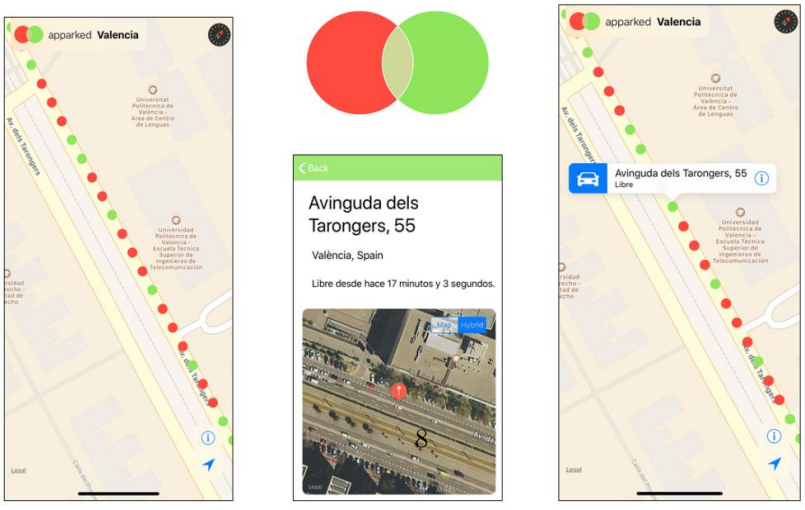

Fig.7. Appearance of the mobile application.

5 Conclusions

The transformation of transport is a reality. New technologies applied to the automotive industry, big data and shared economy are changing the way people approach the world of transport. These advances, which are expected to contribute to an increase in the vehicle fleet together with the growth of the world population, will soon result in unsustainable traffic in the main cities if no actions are taken in this regard. Therefore, the need to have greater control over vehicles is increasing, which is why the design of applications and tools to facilitate user mobility and traffic management emerges as a priority in our days within the intelligent systems of transportation (ITS).

All of the above implies continuous installation and improvement of the current road infrastructure, which is constantly redefining itself. Only a few years ago, the current infrastructure was limited to only physical components such as barriers, traffic lights and traffic regulators. However, the future road infrastructure will be forced to include components such as wireless networks, artificial intelligence and new sensor prototypes to adapt to the current technological changes. In addition, as roads cover a large proportion of the earth's surface, especially within cities, the expected future is that the large number of emerging technologies can turn this element, now passive, into something much more productive.

This above consideration is the main reason why the creation of applications related to IoT and the concept of Smart Cities has currently become a field of much interest in ITS. In the very near future, it is expected to have a lot of information coming from a great variety of sensors, but this must be properly treated to turn it into a useful data. This was the reason why we chose to implement a system by means of magnetic loops that takes advantage of the signals they provide in order to transform them into a very useful mobile application with simple and daily information to the user.

Although road infrastructure has changed significantly in recent years due to the continuous evolution of the technology, the truth is that magnetic loops continue to be the standard traffic sensor. Currently, loop detectors still dominate traffic installations and are even part of the newest algorithms for traffic management in cities. Moreover, these detectors have proven to be very cost effective and truly complete sensors since aside from their main application of vehicle classification, which includes buses, trucks, cars, motorcycles and even bicycles, magnetic loops are also used for vehicle speed measurements, wheel detection, bidirectional communication between vehicles and infrastructures and vehicle re-identification. Therefore, it seemed reasonable to design a system using this technology.

Finally, it should be noted that with the implementation of this application, users would have information on parking spaces in real time, which would help reduce the number of vehicles on the roads and the extensive time spent behind the wheel. In this way, it would also contribute to reducing the pollution of the main cities and the economic losses derived from traffic jams. Consequently, it has been shown that by combining different technologies that are already in operation, it is possible to create very interesting and useful applications for people who live in urban environments.

References

1. Dirección General de Tráfico, «Estadísticas e Indicadores,» 2016.

2. INRIX, «INRIX Global Traffic Scorecard,» 2018. Available: http://inrix.com/scorecard/.

3. INRIX, «Europe's Traffic Hotspots: Measuring the Impact of Congestion in Europe,» 2018.

4. F. Mocholí Belenguer, A. Mocholí Salcedo, V. Milián Sánchez, and J.H Arroyo Núñez. Double magnetic loop and methods for calculating its inductance. Journal of advanced transportation (Hindawi). 2018.

5. F. Mocholí Belenguer, A. Mocholí Salcedo, A. Guill Ibañez and V. Milián Sánchez. Advantages offered by the double magnetic loops versus the conventional single ones. PLoS One. 2019.

6. A. Klein Lawrence, K. Mills Milton, R. P Gibson David. Traffic Detector Handbook. FHWAHRT-06-108. Federal Highway Administration, U.S Department of Transportation 2006.

Development of a 3D spatial sound tool

Ferran Mocholí Belenguer[1], Salvador Borja Ripoll[1], and Antonio Mocholí Salcedo[1]

[1] Instituto ITACA, Universitat Politècnica de València, Camino de vera s/n
46022 Valencia, Spain

fermocbe@upv.es
salva11062@gmail.com
amocholi@eln.upv.es

Abstract. This paper presents a graphic tool designed with Matlab capable of recreating a spatial audio system in real time by listening with headphones. The inclusion of spatial information will allow the listener to identify and select different virtual positions of the sound sources. This incorporation of this spatial sensation will be obtained by filtering the audio signal with special filters, whose frequency response is called Head-Related Tranfer Function, and to perform this filtering in real time, the efficient method Overlap-Save will be used.

1 Introduction

In this technological era full of constant progress in which we live, our lives are increasingly governed by the computers and their respective software, which has favored the emergence of technological breakthroughs, perceived today for example in the proliferation of smartphones and wireless networks.

Within these developments, the audio signal processing has experienced a significant growth in recent years. The constant need to add new sound effects and enhance the feeling of listening has increased the development, research and economic investment in this area, being one of the most significant developments the incorporation of spatial information in audio.

This incorporation of spatial sound in different applications has been mainly driven by virtual and audiovisual environments, such as the video game industry, whose main purpose was to provide a greater sense of reality and immersion. Nevertheless, new 3D sound techniques are also being applied to other very different areas.

It is well-known that human hearing is a delicate and complex process, since the human brain has to combine the information received by both ears to interpret it. However, the information received from each ear is generally different (except when they are equidistant from the source and there is direct vision in both ways). Then, the three-dimensional sensation is related to the difference in amplitude and time received

C.Fernandez-Llatas and M.Guillen (Ed.):
Workshop on Innovation on
Information and Communication Technologies
(ITACA-WIICT 2019)

ISBN 978-84-09-17526-0

by each ear due to the path difference [1]. For this reason, to achieve a virtual location of the sources, we will need to process the information from each ear separately, which commonly is known as L and R channels, comparing the phase and amplitude between two signals.

With the above, the objective of this work will intend to implement a tool capable of generating spatial sound in real time through a very simple and didactic user interface developed through the concatenation of graphic interfaces. To achieve this purpose, which includes filtering and reproduction of audio signals in real time, PlayRec libraries have been used [2], since they allow easy access to sound cards and create buffers that store information. The result is that the signals are processed while the previously processed ones are reproduced. Finally, this 3D effect will be accomplished by using a series of FIR filters, commonly called head-related impulse responses in time domain or head-related transfer functions in frequency domain.

2 Binaural reconstruction systems

Human brain uses the characteristics of interaural time (ITD) and interaural level difference (ILD) to locate a sound source. Therefore, binaural reconstruction systems are based precisely on the idea that although the sound scene is very complex, the listener will only capture from it what comes to their ears. Consequently, it seems logical to design a system that reconstructs exactly the signal that finally reaches the ears of the listener, which involves providing the exact values of ITD and ILD under certain characteristics.

The ITD and the IDL are complementary, while the ITD works well below 1.5 KHz, the ILD does it above this frequency [3]. However, the use of the ITD and ILD values do not allow to locate a sound source in elevation. It was therefore necessary to wait until the 1960s for the definition of the Head Related Impulse Response (HRIR) or its frequency version called Head Related Transfer Function (HRTF). This includes all the physical aspects of the location of the sound for a specific position of the head such as interaural time difference, shadow of the head and diffraction in the ear, and is measured by placing two small microphones in the ears of the listener and recording for all the desired elevation positions and azimuth the signal contribution that reaches each ear.

Thus, once the behavior of each ear is known, binaural sounds can be artificially generated by filtering the signal from a sound source recorded in anechoic conditions with the different filters of the HRTF [4]. In general, this process is done in the domain of the frequency through DFT's and its efficient FFT algorithm, since filtering is faster than in the time domain. In addition, as our sound tool will work in real time, the computing cost will be crucial. Consequently, the Overlap-Save filtering method will be used.

3 Digital Filtering

In our 3D spatial sound tool, we will work with a system that will filter digital audio files as seen in Figure 1. Therefore, our system will be:

- Discrete in time.
- Invertible.
- Causal.
- Stable.
- Invariant in time.
- Linear.

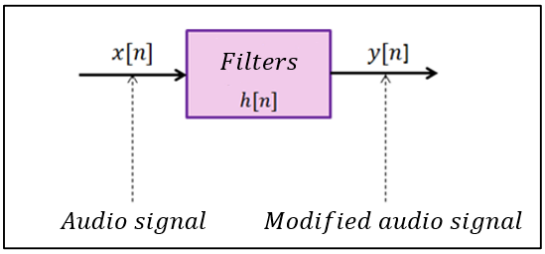

Fig. 1. Audio system characterization.

When we model a discrete-time system, the input is a certain signal $x\,[n]$, which after passing through a system characterized by a response to the impulse $h\;\;[n]$, is transformed into an output $y\,[n]$. The relationship between $y\,[n]$ and $x\,[n]$ is as follows:

$$y[n] = \sum_{k=-\infty}^{\infty} x[k]h[n-k] = x[n] * h[n] \tag{1}$$

The convolution is a mathematical operation that uses the symbol * and combines two signals to produce a third signal [5], thus allowing the output signal of a system to be obtained from the input signal and its impulse response. Then, as our system will filter an audio signal $x\,[n]$ through different FIR filters ($h_1[n]$ and $h_2[n]$) extracted from the HRTF to emulate that the sound comes from different locations, the previous block diagram would look better as in Figure 2 and Equation 1 could be rewritten as:

$$\begin{aligned} y_1[n] &= x[n] * h_1[n] \\ y_2[n] &= x[n] * h_2[n] \end{aligned} \tag{2}$$

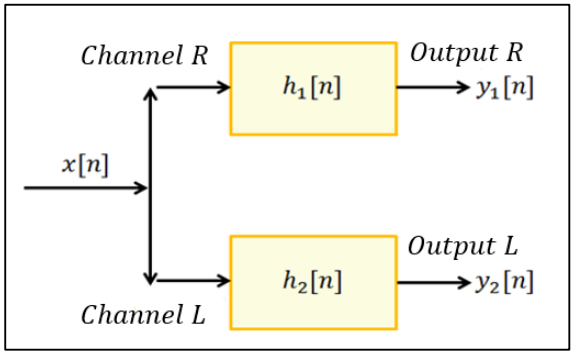

Fig. 2. Signal diagram in a stereo audio system.

However, one of the most important properties extracted from the Fourier transforms applied to the LTI systems described above, comes from the property of the convolution, which expresses that if $X(e^{j\omega})$ is the Fourier transform of $x[n]$ and $H(e^{j\omega})$ is the Fourier transform of $h\,[n]$, there is a relationship between both domains:

$$y[n] = x[n] * h_1[n] \qquad <-> \quad Y(e^{j\omega}) = X(e^{j\omega}) \cdot H(e^{j\omega}) \tag{3}$$

Then, there is a direct relationship between the signals in time and their respective transformed in the frequency domain. In this way, the output of the system will be the convolution of the input signal and the impulse response in time domain or the multiplication of these ones in frequency domain. Figure 3 shows all possible ways to perform this filtering.

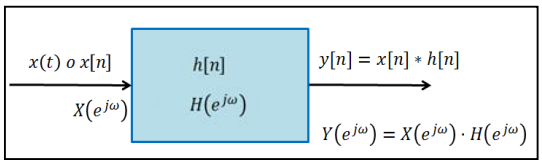

Fig. 3. Audio system characterization.

4 Fourier transform

The DFT is a type of discrete transform used in Fourier analysis that transforms one mathematical function into another. The original function must be a function in the time domain and the result obtained is a representation of it in the frequency domain.

Since the input of the DFT is a finite sequence of real or complex numbers, it is ideal for processing information stored in digital media. In fact, in addition to being used in digital processing and other fields related to the frequency analysis of signals, is also widely useful to solve differential equations and carry out operations such as convolutions or multiplications of long integers.

A very important factor for this type of applications is that the DFT can be calculated in practice in a very efficient way by using the algorithm of the Fast Fourier Transform (FFT). Indeed, it is so common to use FFT to calculate DFT's that the term "FFT" is often used to refer to "DFT".

According to the formula of the DFT, it would require approximately one million operations to calculate a DFT of size N = 1000, being N the period of the DFT (the number of computational operations for said transformation is given by N^2). However, this number could be reduced to approximately 7,000 operations if the FFT is used, since in this case, the number of operations is given by $N\ log\ (N)$, especially if N is a power of two.

Therefore, our objective will be to perform the convolution of $[n]$ with $h\ [n]$ using the FFT algorithm to save a large number of operations and therefore, a large computational cost, which could complicate our real-time system.

5 Overlap-Save

When the convolution is performed by using the FFT, we are actually applying the circular convolution. Thus, in this method each block will be composed of samples from the previous block and new samples.

Specifically, the Overlap-Save [6] method consists of the following:

- The signal to be filtered $x[n]$ is divided into independent blocks of size L, where $L = N - P$, being P the filter size.
- The DFT of size N of the impulse response of the filter $h\ [n]$ is calculated.
- For each block of $x\ [n]$:
    1. Add P samples from the previous block.
    2. The DFT of size N of the block is calculated.
    3. Multiply element to element this DFT by the DFT of the filter.
    4. The inverse DFT of size N is calculated.

5. The P first samples of each block are discarded to obtain L valid samples.

- The calculation is finished when at least $Lx + (P - 1)$ samples from $[n]$ are obtained, being Lx the length of $x\,[n]$.

In our particular case, we will divide the signal into independent blocks of size L = 512 and the filter size will also be P = 512 samples. Following the formula of the first point, the size of the DFT will therefore be N = 1024. Consequently, in each block of $x\,[n]$ we will have a total of 1024 samples, 512 new (L) and 512 samples from the previous block (L'). Next, the different DFTs applied to $x[n]$ and a $h\,[n]$ will be multiplied point by point. Once we have the $y[n]$ in the frequency domain, we will apply the inverse DFT to retrieve $y[n]$ in the time domain. Finally, we will discard the first 512 samples of this one. Figure 4 shows a scheme for a better understanding.

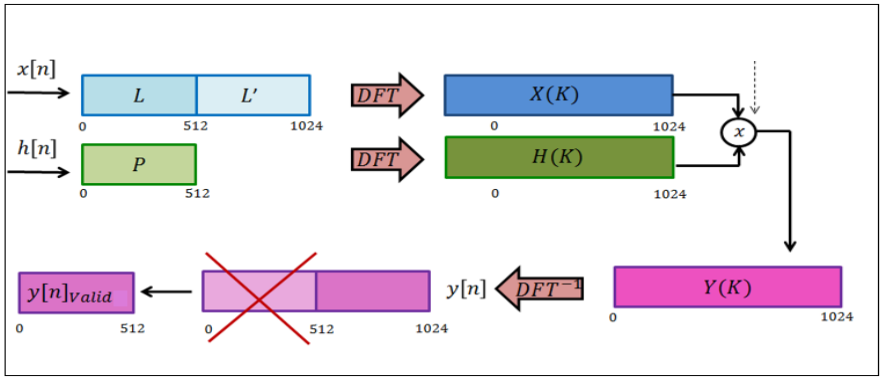

Fig. 4. Overlap - Save method.

6 Spatial sound tool

All this signal processing is derived in a very simple audio tool composed of several graphic interfaces. It starts with an interface like the one shown in Figure 5, in which the user must choose the sex and press 'Start'. Depending on the chosen sex, a HRTF [7] from a male or a female will be taken.

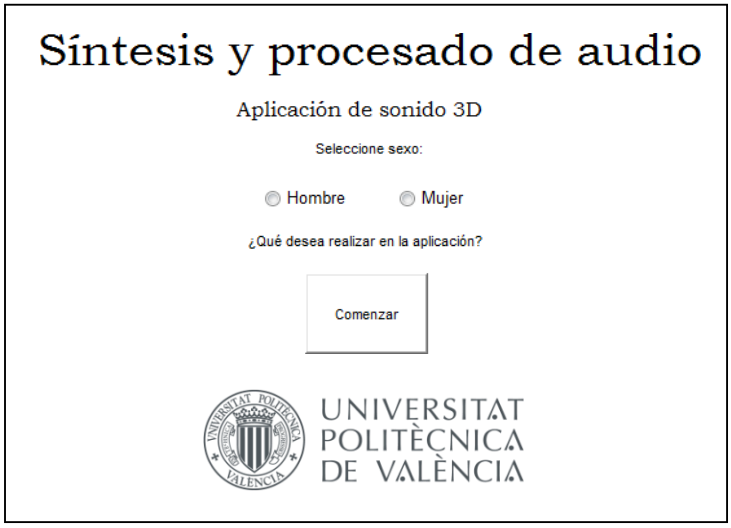

Fig. 5. Initial interface.

In the following interface, the users must choose if they want to work with mono audio or stereo audio as shown in Figure 6.

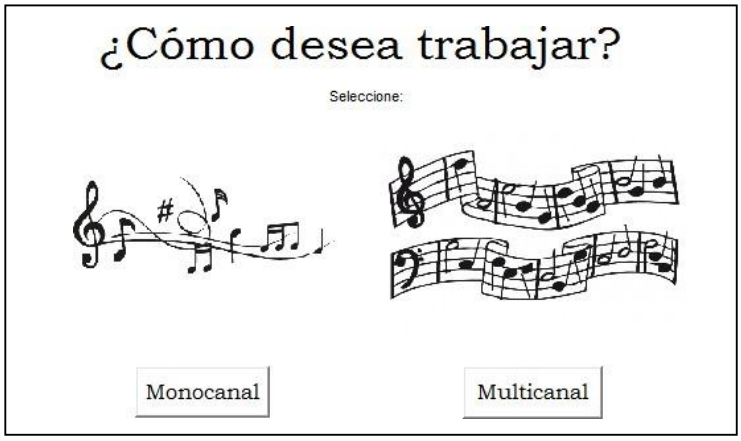

Fig. 6. Interface to choose audio type.

If stereo audio is chosen, an interface like the one shown in Figure 7 will be displayed, in which the user will be able to select different positions for the violin and the piano.

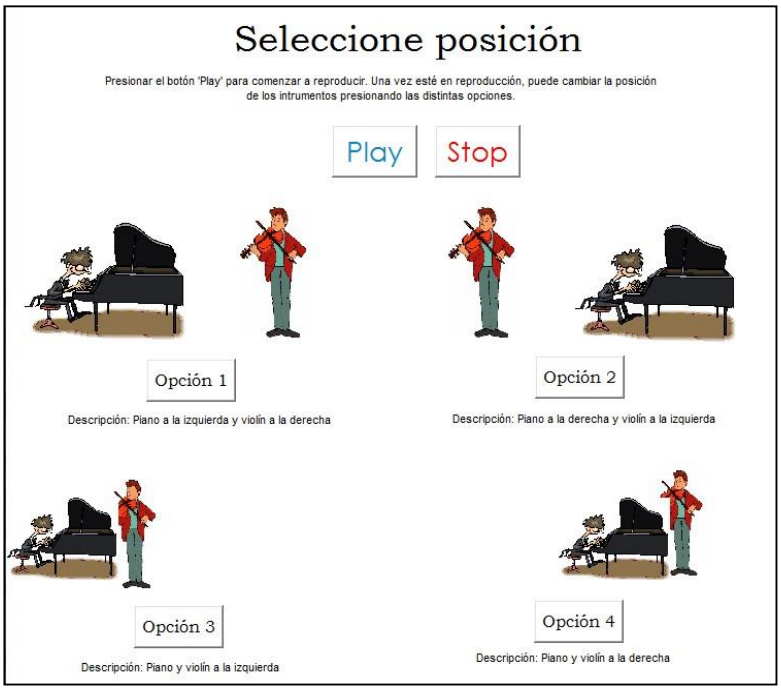

Fig. 7. Multichannel interface.

However, if the choice is mono audio, the interfaces of Figure 8 and Figure 9 will be opened. In these, the user can select the type of audio and vary its origin in real time.

Fig. 8. Interface to choose the type of mono audio.

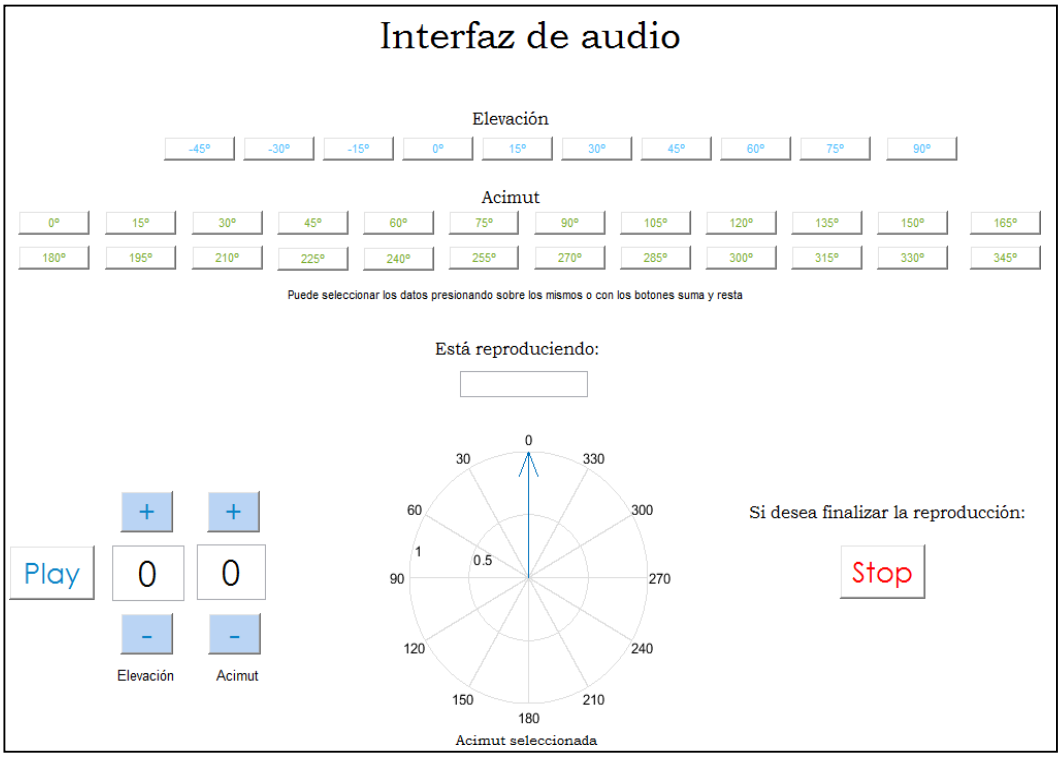

Fig. 9. Main interface.

References

1. Mocholí Belenguer, Ferran. Desarrollo y evaluación de técnicas de audio espacial. Septiembre 2014. Universidad Politécnica de Valencia.

2. Robert Humphrey. PlayRec – Multichannel Matlab Audio. Enero 2006. Proyecto de la Universidad de New York.

3. Antonio Belloch, Miguel Ferrer, Alberto Gonzalez, Jorge Lorente y Antonio M.Vidal. GPU-based systems with mobile Virtual Sound Sources and Room Compensation. Septiembre 2013. Universidad Politécnica de Valencia.

4. Antonio Belloch, Miguel Ferrer, Alberto Gonzalez, F.J. Martinez-Zaldivar y Antonio M.Vidal. Headphone-Based Virtual Spatialization of Sound with a GPU Accelerator. Julio 2013. Universidad Politécnica de Valencia.

5. José Morón. Señales y sistemas. Enero 2011. Fondo Editorial Biblioteca Universidad Rafael Urdaneta.

6. Don Davis & Euegene Patronis Jr. Sound System Engineering, Third Edition. Editorial Focal Press. 2006

7. Recherche Ircam - Instituto francés de investigación y coordinación de audio y música. HRTF Database. France, 2006.

Preliminary study of the relation between FIFA standard tests and football players' perception in artificial turf pitches

Luis I. Sánchez-Palop[1], José Fco. Pedrero-Sánchez[1], Mario Aguado-Virseda[1], Enrique Alcántara-Alcover[1], Sabina Asensio-Cuesta[2], José Laparra-Hernández[1], Fernando Gómez-Sendra[1], Rafael Mengual-Ortolà[1].

[1] Instituto de Biomecánica de Valencia (IBV), Universidad Politécnica de Valencia, Camino de Vera s/n, 46022, Valencia, Spain

[2] Instituto de Tecnologías de la Información y Comunicaciones (ITACA), - Universitat Politècnica de València, Camino de Vera s/n. 46022 Valencia, Spain

Abstract. FIFA tests to assess the properties of artificial turf surfaces, established to certificate the quality of football fields, are the current standard to evaluate field conditions. The objective of this study is to analyze whether there is a correlation between the results of the standard tests and the subjective perception of football players about the field suitability to play football (playability). A combination of objective (FIFA standards) and subjective (ability tests and perception questionnaire) tests was performed in three different fields with different surface conditions. The comparison of the results obtained from both tests showed a discrepancy, outlining the interest of further research to improve standard tests.

Keywords: Turf, tests, perception, playability, football fields.

1. Introduction and scope of the project

In 2019, football is one of the most common sports worldwide. Up to 211 countries are currently members of the FIFA board, the overall governing body of recognized international football.

Traditionally, natural grass has been the only surface to play elite football, but the reality is that, some countries have climate conditions that make extremely difficult and costly to maintain the grass. In the 2004/2005 season, FIFA changes the laws of the game to allow playing elite football also in 3rd generation artificial turf (also called 'football turf').

However, even if the acceptance among professional players has increased, and more and more countries are adopting artificial turf due to its economic advantages and climate independence, but the initial resistance is still present.

An 18-month study carried out by FIFA [7] in the second half of the 2010/2011 season among 1,129 elite players of 44 different countries around the globe pointed out that the footballers' perception was rather negative on artificial turf fields. The findings included a higher variation of the field conditions for artificial than natural surfaces and

C.Fernandez-Llatas and M.Guillen (Ed.):
Workshop on Innovation on
Information and Communication Technologies
(ITACA-WIICT 2019)

ISBN 978-84-09-17526-0

a higher perception of injury risk and tiredness. However, almost the 60% of the footballers agreed that they "would rather play on a modern artificial pitch than a poor quality natural pitch".

To ensure the fields present at least a minimum level of mechanical properties, FIFA established their Handbook of Test Methods [8] and Handbook of Requirements [9], which include the testing methodologies and approved values for properties such as traction, impact absorption, deformation, ball roll, ball rebound, regularity, etc.

Several studies have already covered the influence of the field physical-mechanical properties (traction, hardness, regularity, abrasiveness, etc.) over the playing actions (what is called playability, and can be summarized as ball and player behavior) [3, 5] and injury risks [11, 15, 17]. All these studies have proved the correlation between the surface characteristics and its impact on the players' and performance by means of objective tests, and they stablish the basis for further analysis.

Other researches have focused in the measurement of the player perception playing in different surfaces. Several studies cover this topic for artificial turf, natural grass and other types of field surfaces he next step forward was to measure the player perception of different surfaces. [2, 4, 12, 13, 17]. These studies approach the subjective measurement of the field properties with the aim of compare artificial and natural turf or different turf surfaces, with fixed questionnaires or interviews where the players could give their opinions freely. The main limitation of these studies is the lack of objective measurements to compare with the subjective results.

Finally, some studies combined the gathering of subjective and objective data, focused mainly in the player-surface interaction (hardness of the ground, traction, etc.) [1, 15].

The present study focuses in the overall playability concept (which involves player-surface, ball-surface and player-ball interactions) and analyses it from the subjective point of view and the objective measurements of the FIFA Standard methods. The main difference in this approach from previous subjective studies is that the main scope of this study is to analyze the adequacy of the standard methods to assess playability, studying the correlation between FIFA tests and the players' perception.

2. Methodology and in-field tests

The study was performed over 3 artificial turf fields, selected according on their current surface state (wear and maintenance of the playing surface). FIFA Quality Programme levels (FIFA Quality Pro and FIFA Quality) [9] were the selection criteria used, ensuring that two fields fell each one in one of these categories, plus a third field under the minimum requirements according to the Programme.

All fields were located in the Valencia area (Spain): Bonrepós i Mirambell (year of installation 2017), Marxalenes (2014) and Doctor Lluch (2010).

The measurements acquisition was organized in two different parts: (1) objective measurements; (2) subjective assessment.

Objective measurements: The objective measurements consisted on a reduced protocol of the FIFA Standard test. Fig. 1 shows the testing points as defined in the FIFA Handbook of Test Methods [8]. Regarding the tests selected, they included Rotation

traction, Shock absorption and Standard deformation (AAA test), Ball roll and Ball rebound, to assess the player-surface and the ball-surface interactions.

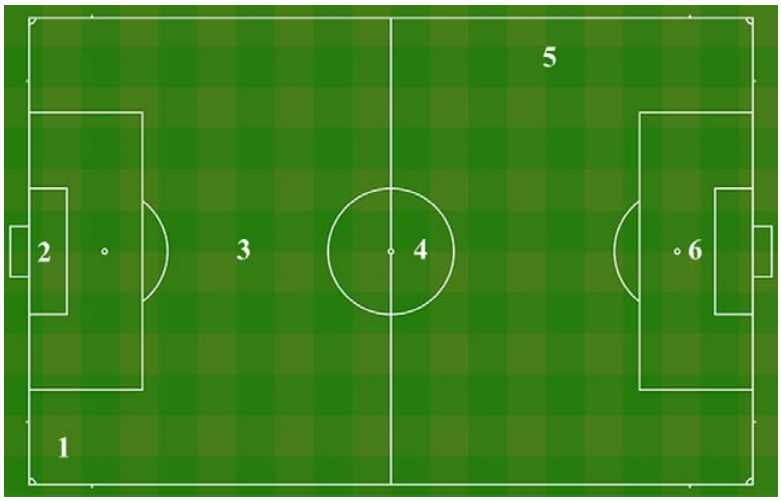

Fig. 1. Testing points as defined in FIFA Handbook of Test Methods

The FIFA established values regarding the tests performed in this study for each field quality level are included in Table 1 [9]. The three levels defined in this study were FIFA Quality PRO (highest certification currently available), FIFA Quality (second best certification) and No Pass (values measured outside the FIFA ranges to certificate a field). The main difference between FIFA Quality Pro and FIFA Quality is that the first reduces the width of the acceptance range, thus the variability allowed between fields is lower.

Table 1. Ranges of acceptability of FIFA standard tests for each FIFA certification levels

Quality	Rotational resistance (Nm)	Shock absorption (%)	Standard deformation (mm)	Ball roll (m)	Ball rebound (m)
FIFA Quality Pro	30-45	60-70	4-10	4-8	0.60-0.85
FIFA Quality	25-50	55-70	4-11	4-10	0.60-1.00

Subjective measurements. In the subjective analysis, 5 youth players (ages ranged from 17 to 18 years old, all field player from different positions – defenseman, left wing, defensive midfielder, offensive midfielder and striker) performed agility tests, and answered a questionnaire afterwards.

The agility test was based on the Illinois Test [10], a commonly used protocol to evaluate athlete's agility, speed and reaction times (Fig. 2). All players completed the circuit with and without a football (3 times each, 6 times in total).

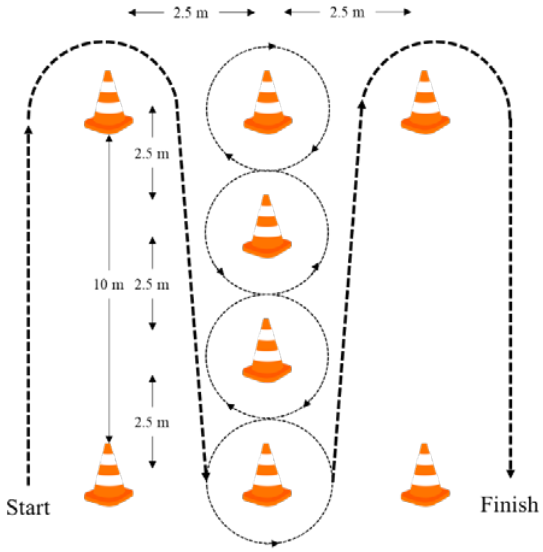

Fig. 2. Illinois Test set-up

After the test was completed, the players had to fulfill a questionnaire with closed questions. Even if open commentaries were recorded, during the design of the questionnaire we opted for closed questions to reduce the effect of the examiner on the results.

Fig. 3. Images of the agility test (right) and the Ball roll standard test (left)

The scale used for the questions present in the questionnaire are included in Table 2. After the analysis of the different parameters of player-surface and ball-surface behavior, players were asked to give an overall score (1 to 10 scale) to each field.

Questions were structured in 2 parameters' categories: (1) *player-surface parameters* (traction, shock absorption and field homogeneity); (2) *ball-surface interactions parameters* (Ball control, Ball predictability and Ball speed).

Table 2. Scores for each question in the questionnaire

Player-surface parameters	**Scale**	**Ball-surface parameters**	**Scale**
Traction (rotational resistance)	1 Extremely low 2 Low 3 Slightly low 4 Average 5 Slightly high 6 High 7 Extremely high	Ball control	1 Extremely difficult 2 Difficult 3 Slightly difficult 4 Average 5 Slightly easy 6 Easy 7 Extremely easy
Shock absorption	1 Extremely soft 2 Soft 3 Slightly soft 4 Average 5 Slightly hard 6 Hard 7 Extremely hard	Ball predictability	1 Extremely irregular 2 Irregular 3 Slightly irregular 4 Slightly homogeneous 5 Totally homogeneous
Field homogeneity	1 Extremely irregular 2 Irregular 3 Slightly irregular 4 Slightly homogeneous 5 Totally homogeneous	Ball speed	1 Extremely slow 2 Slow 3 Slightly slow 4 Average 5 Slightly fast 6 Fast 7 Extremely fast

Each field was tested in a separate day, to avoid tiredness as a factor. On the other hand, by splitting the testing days it should be harder for the players to compare between fields, thus the ratings could be independent for each surface.

3. Results

FIFA tests. The first part of the study consisted in the analysis of the objective measurements from the FIFA standard tests to check the validity of the fields selected. Table 3 shows the mean and the standard deviation for each test and field, along with the FIFA Quality Programme level (according to the values on Table 3) [9].

It is possible to conclude that the field selection was adequate. The most recently installed field (Bonrepós i Mirambell) outperformed the middle aged (Marxalenes) and the older (Doctor Lluch) fields, and almost all its results were within the FIFA Quality

Pro standards. Only the Ball rebound fell into the second category (FIFA Quality), but still, its results were better.

The medium field (Marxalenes) fell in the middle of the other two fields, and presented FIFA Quality levels for Rotational resistance, Ball roll and Ball rebound. Its Shock absorption and Standard deformation values were within the FIFA Quality levels. However, its Shock absorption was worse than the measure of Bonrepós i Mirambell and presented a higher dispersion, and the Ball roll was in the edge between FIFA Quality Pro and FIFA Quality (8 m).

Finally, the oldest field was also the worst in terms of performance. It did not reach the FIFA Quality ranges of acceptance for none of the tests except the Standard deformation. Nevertheless, the lack of shock absorption of the surface explains the good performance in terms of deformation, both measured in the same test (AAA test), as they are related. A higher surface capacity to absorb impacts usually comes with a higher deformation. The optimal performance requires a tradeoff between both parameters: an excessive hardness will result in a higher risk of injury, but a higher deformation will also increase the risk as it increases the instability of the gait [6, 14].

Table 3. Results of the standard tests (mean and standard deviation) for each field and FIFA qualification of the results

Field		**Rotational resistance (Nm)**	**Shock absorption (%)**	**Standard deformation (mm)**	**Ball roll (m)**	**Ball rebound (m)**
Bonrepós I Mirambell	Mean	39.0	61.98	9.1	7.3	0.95
	Sd.	3.2	1.62	0.4	0.3	0.03
	FIFA Level	Quality Pro	Quality Pro	Quality Pro	Quality Pro	Quality
Marxalenes	Mean	45.2	61.54	8.4	8.9	0.98
	Sd.	2.2	4.23	0.8	1.2	0.04
	FIFA Level	Quality	Quality Pro	Quality Pro	Quality	Quality
Doctor Lluch	Mean	48.4	51.66	6.0	13.3	1.15
	Sd.	3.2	0.55	0.0	1.0	0.01
	FIFA Level	No Pass	No Pass	Quality Pro	No Pass	No Pass

Agility test and questionnaires. Regarding the subjective assessment, Table 4 presents the mean score and the standard deviation of the results for each question

Table 4. Descriptive analysis of the questionnaires

Field		Traction	Shock absorption	Field homogeneity	Ball control	Ball predictability	Ball speed	Overall score
Bonrepós	Mean	5.0	5.0	3.2	3.8	3.6	2.2	6.4
	SD	1.2	1.2	1.1	1.3	0.5	0.4	0.5
Marxalenes	Mean	4.0	3.4	4.6	7.0	4.8	4.0	9.2
	SD	0.0	1.1	0.5	0.0	0.4	1.2	0.4
Dr. Lluch	Mean	5.6	5.6	2.4	3.6	3.0	4.6	4.0
	SD	1.5	1.5	0.5	1.1	1.0	1.3	1.0

It is interesting to divide the questions in player-surface (traction, shock absorption and field homogeneity) and ball-surface interactions (Ball control, Ball predictability and Ball speed), and afterwards to analyze the Overall score to check if it is coherent with the rest of the ratings.

Fig. 4, Fig. 5 and Fig. 6 represent the mean score for each question and field in a linear scale to ease the comprehension of the answers given by the footballers.

Regarding the *player-surface parameters*, some discrepancies between the objective tests and the players' perception arose. As showed in Fig. 4, the fields of Bonrepós i Mirambell and Marxalenes swapped positions, as the medium quality field (Marxalenes) was the best rated. No disagreement between objective and subjective results appeared for Dr. Lluch, the oldest and lowest quality field, which was perceived as the worst-performance field among the three.

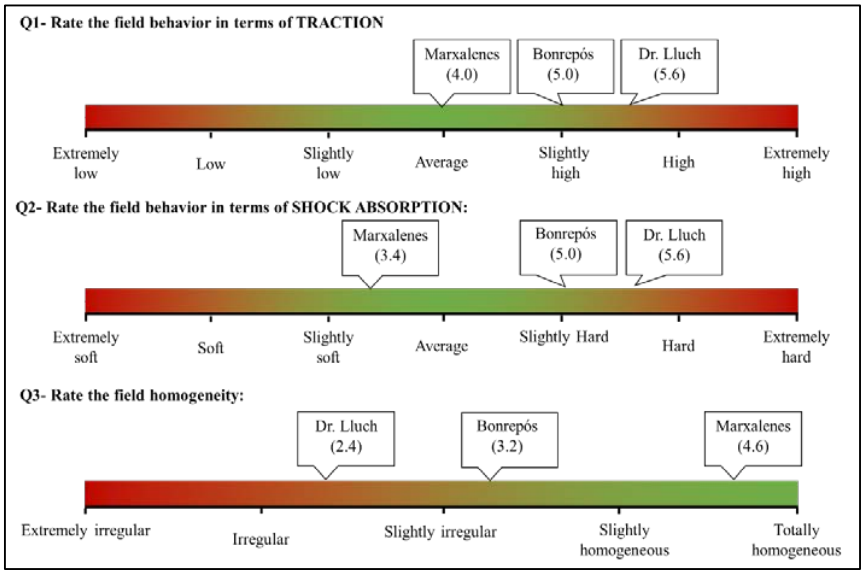

Fig. 4. Mean scores for each field for the player-surface related questions

As for the *ball-surface parameters*, Fig. 5 presents the same deviation from the objective tests. Dr. Lluch is still the lowest rated field, except for the Ball speed, and Marxalenes the highest rated for all parameters.

A further analysis of the *ball-surface parameters* should consider that all three are related. In this case, the possible explanation of the ratings could be linked to the fields the subjects of the study usually play football. As youth players, they are used to play in field whose surfaces are more likely to be the same as Marxalenes, and a similar maintenance conditions.

This factor might be especially relevant for Ball control and Ball speed (as predictability should be more related to the homogeneity of the field surface). The hypothesis to explain the results obtained is that the subjects of the study found the surface of Bonrepós I Mirambell as too slow (the objective test of Ball roll agreed as Bonrepós was the field with the shortest distance travelled by the ball) with respect to the surfaces they usually play.

This result outlines one limiting factor of the Ball roll FIFA test, especially on how it ranks the fields according to the distance travelled by the ball. The current FIFA Quality Pro and FIFA Quality levels (Table 1) considers the total distance from the slope used to release the ball to the final position of the ball when it completely stops. The acceptability bands are 4-8 meters for FIFA Quality Pro and 4-10 for FIFA Quality, but the results of this study might suggest that these limit should be reconsidered, as players felt more comfortable playing football in the field with values of Ball roll test of around 9 meters (Marxalenes) than 7 meters (Bonrepós I Mirambell).

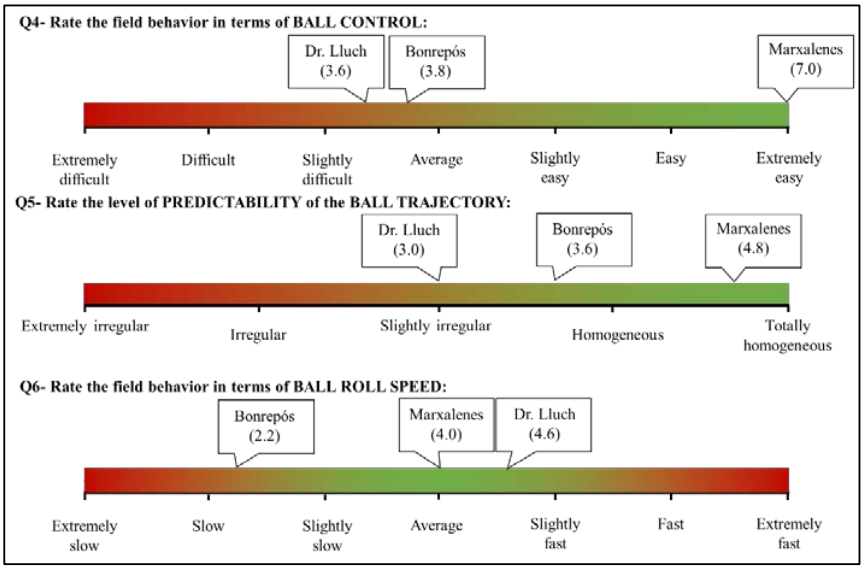

Fig. 5. Mean scores for each field for the ball-surface related questions

The overall rating of each field (Fig. 6.) agreed with the specific ratings for each question, as the order of preference was Marxalenes (9.2), Bonrepós i Mirambell (6.4) and Dr. Lluch (4.0).

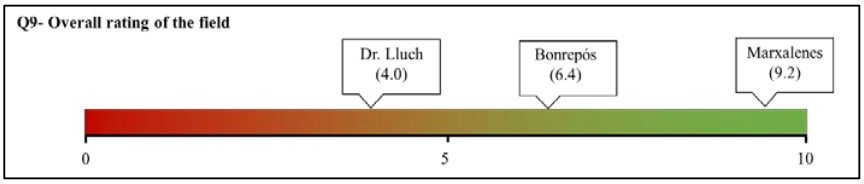

Fig. 6. Overall scores for each field

From a statistical point of view, a post-hoc Kruskal-Wallis analysis has been carried out to analyze if there are differences between the fields (one-on-one comparisons) in the results of the questionnaire. Table 5 shows that the main differences appeared between Marxalenes and the other two fields (results in concordance with the previously discussed ratings and figures).

Going into detail, the greatest statistical differences appear for the *ball-surface parameters* between Bonrepós-Marxalenes, and Marxalenes-Dr. Lluch. For both comparisons, Ball control and Ball predictability are different, and Ball speed differences are significant for Bonrepós-Marxalenes and Marxalenes-Dr. Lluch. It is important to note that Marxalenes was the field in the middle for the Ball roll test, while Bonrepós had the lowest values of distance travelled by the ball (thus it is expected to be the slower field in terms of all speed) and Dr. Lluch the highest values (hence, the fastest field).

The *player-surface* differences are more important between Marxalenes-Dr. Lluch (for Shock absorption and Field homogeneity), whereas between Bonrepós-Marxalenes only Field homogeneity present statistical differences.

The *player-surface* interaction parameters do not present great differences between the fields, which are mainly found in the *ball-surface parameters*. This could happen because the dispersion of the ratings is wider for the player-surface parameters, as it is more difficult to identify and isolate the surface behavior (they depend also on the footwear used, the gait of the player, his biomechanics, etc.). On the other hand, the *ball-surface parameters* are more easily evaluable as they only depend on the surface and the ball.

Table 5. Significance levels for the Kruskal-Wallis test between fields

Parameter	Traction	Shock absorption	Field homogeneity	Ball control	Ball predictability	Ball speed	Overall score
Bonrepós-Marxalenes	0.092	0.068	0.049*	0.005*	0.014*	0.012*	0.006*
Bonrepós-Dr. Lluch	0.262	0.262	0.166	1.000	0.307	0.009*	0.008*
Marxalenes-Dr. Lluch	0.090	0.042*	0.007*	0.005*	0.012*	0.439	0.007*

** refers parameters with significant differences ($p<0.05$)*

4. Conclusions and future development

The main conclusion that can be drawn from the results of this preliminary study is that there might be a certain discrepancy between the evaluation of the field obtained from the current standard tests and the players' perception. This deviation appeared especially with the *ball-surface parameters*, and it could be caused by the different perception of what an optimal ball speed should be. The current Ball roll test only measures the distance travelled, and this could be rather limiting, as it is not clear that a shorter distance (and thus a slower speed) is better.

This conclusion, however, has to be validated in a deeper study with a wider sample of players and fields. The subjects of this study were only 5 and from the same team and competition level, thus their perception on the ball behavior would probably be biased by the behavior of the fields where they usually play.

Nevertheless, there is a conclusion that does not depend on the ratings obtained from the results regarding the evaluation of the *ball-surface* properties. The current standard test only contemplate the Ball roll and the Ball rebound. However, the behavior of the ball during the playing actions also depend on factors such as the homogeneity or regularity of its trajectory.

Considering both results, we propose further research to develop testing methodologies that measure more accurately the behavior of the ball, mimicking the actions that occur during the actual football games.

On behalf of the *player-surface* performance of the fields, the results of the standard tests are closer to the player's perception. Still, as aforementioned, it is important to note that the perception might be influenced by external factors such as the footwear, whereas the ball-surface performance is more easily evaluable.

References

1. Aldous. D. E.; Chivers. I. H.; Kerr. R.: Player perceptions of Australian Football League grass surfaces. International Turf grass Society Research Journal 10. 318-326 (2005)
2. Andersson. HA. Ekblom. B. Krustrup. P.: Elite football on artificial turf versus natural grass: Movement patterns, technical standards and player impressions. Journal of Sports Sciences. 1-10 (2007)
3. Bell. MJ. & Holmes. G.: The playing quality of association football pitches. Journal of the Sports Turf Research Institute. 61. 19-47 (1988)
4. Burillo. P. Gallardo. L. Felipe. JL. & Gallardo. A. M.: Artificial turf surfaces: Perception of safety, sporting feature, satisfaction and preference of football users. European Journal of Sport Science. 14 (Suppl. 1). 437-447 (2014)
5. Canaway. PM. Bell. MJ. Holmes. G. Baker. SW: Standards for the playing quality of natural turf for Association Football. West Conshohocken. PA: American Society for Testing and Materials (1990)
6. Ekstrand. J. Timpka. T. Hägglund. M.: Risk of injury in elite football played on artificial turf versus natural grass: a prospective two-cohort study. Br J Sports Med 40. 975-980 (2006)
7. FIFA: Elite platers' perception of football playing surfaces. FIFA Quality Programme for football turf (2012)
8. FIFA: Handbook of test methods. FIFA Quality Programme for football turf (2015)
9. FIFA: Handbook of requirements. FIFA Quality Programme for football turf. (2015)
10. Getchell B.: Physical Fitness: A Way of Life. 2nd ed. New York: John Wiley and Sons. Inc. (1979)
11. Poulos. C. Gallucci. J. Gage. WH. Baker. J. Buitrago. S. Macpherson. AK: The perceptions of professional soccer players on the risk of injury from competition and training on natural grass and 3rd generation artificial turf. BMC Sports Science. Medicine and Rehabilitation. 6:11 (2014)
12. Roberts. J. Osei-Owusu. P. Harland. A. Owen. A. Smith. A.: Elite football players' perceptions of football turf and natural grass surface properties. Procedia Engineering 72. 907-912 (2014)
13. Ronkainen. J. Osei-Owusu. P. Webster. J. Harland. A. Roberts. J.: Elite player assessment of playing surfaces for football. Procedia Engineering 34. 837-842 (2012)
14. Rosa D. Sanchís M. Alcántara E. Zamora T. (2007) Avances en el estudio de campos de hierba artificial. aportaciones biomecánicas. Biomecánica aplicada a la actividad física y al deporte (pp. 405-429). Ayuntamiento de Valencia.
15. Straw, CM. Samson, CO. Henry, GM. Brown, CN: Does variability within natural turf grass sports fields influence ground-derived injuries? European Journal of Sport Science (2018)
16. Wright. JM. Webner. D: Playing field issues in sports medicine. Sports Med. Rep. Vol. 9. No. 3. pp. 129-133 (2010)
17. Zanetti. EM: Amateur football game on artificial turf: Players' perceptions. Applied Ergonomics 40. 485–490 (2009)

Comparison of an Improved Matrix-based Error Correction Code*

J. Gracia-Morán[1], L.J. Saiz-Adalid[1], D. Gil-Tomás[1], J.C. Baraza-Calvo[1], P.J. Gil-Vicente[1]

[1] Instituto ITACA. Universitat Politècnica de València. Camino de Vera s/n. 46022 Valencia, España.
{ jgracia, ljsaiz, dgil, jcbaraza, pgil } @ itaca.upv.es

Abstract. Nowadays, the probability of occurrence of *Single Cell Upsets* (SCUs) or *Multiple Cell Upsets* (MCUs) has increased due to the continuous increment in the integration scale of CMOS technology, that has provoked an augment in the fault rate. SCUs and MCUs are particularly common in computer memory systems. To tolerate errors, it is common the use of Error Correction Codes (ECCs). Nevertheless, when using ECCs, a series of overheads are added: extra bits to detect and/or correct errors, and some area, power consumption and delay overheads of the encoders and decoders circuits.
In order to tolerate MCUs, different approaches have been presented in the literature. Specifically, in this work, we present a complete comparison of different matrix-based ECCs, some of them recently presented.

1 Introduction

Nowadays, with the aggressive size reduction of CMOS technology, memory systems provide a large storage capacity. This aggressive scaling has provoked also an augment in the memory error rate [1], [2]. Thus, the impact of a cosmic radiation particle can provoke the change in a single memory cell (known as *Single Cell Upset* or SCU), or in several memory cells (*Multiple Cell Upsets* or MCUs). An MCU can be defined as simultaneous errors in more than one memory cell induced by a single particle [3], [4], [5], [6], [7].

A possible protection method for memories are Error Correction Codes (ECCs). Traditionally, common ECCs used have been SEC or SEC-DED codes [8], [9], [10]. SEC codes can correct an error in a single memory cell, while SEC-DED codes can correct an error in a memory cell, as well as they can detect two errors in two independent cells.

As the number of errors increases, error coverage of the added ECCs should also increase. For example, in critical applications, more complex and sophisticated codes are used [11], [12], [13], [14], [15], [16], [17], [24]. We have focused on matrix-based

* This work has been partially funded by the Spanish Government under the project TIN2016-81075-R and by Primeros Proyectos de Investigación (PAID-06-18), Vicerrectorado de Investigación, Innovación y Transferencia de la Universitat Politècnica de València (UPV), under the project 200190032.

C.Fernandez-Llatas and M.Guillen (Ed.):
Workshop on Innovation on
Information and Communication Technologies
(ITACA-WIICT 2019)

ISBN 978-84-09-17526-0

codes [14], [15], [18], [28], [29] for their ease of implementation, which causes a low overhead, and the possibility of adapting these codes to different types of errors. Some examples are the works presented in [15] and [18]. Column-Line-Code (CLC code) [15] combines extended Hamming codes (a SEC-DED code) and parity checks to correct different error patterns. On the other hand, FUEC-M [18] organizes the data bits in a bi-dimensional way, and uses a unique ECC to tolerate adjacent faults.

Nevertheless, several factors must be considered when an ECC is included in memory systems. Firstly, a number of extra bits (called also redundant or code bits) are stored together with each data word, as these redundant bits are used to detect/correct the possible errors occurred. Thus, the number of code bits should be as low as possible. For example, if an ECC with 100% of redundancy is used in a 2GB memory, only 1GB will be available to store the "clean" data; the remaining 1GB is required for the code bits.

Secondly, the circuits that generate the code bits and check if there is an error will introduce some area, power consumption and delay overheads.

In a previous work [18], we presented a new Matrix-based ECC, called FUEC-M. This ECC presents a low redundancy, while improves the error coverage with respect to other Matrix-based ECCs. FUEC-M is designed to correct a series of adjacent error patterns. In [30], we have improved FUEC-M in order to enlarge its error correction capabilities. This new ECC, called FUEC-ME, allows the correction of a bigger set of adjacent errors, but maintaining the same redundancy than FUEC-M.

In this paper, we complete the comparison presented in [28]. Specifically, we have compared CLC code [15], FUEC-M [18] and FUEC-ME [30], studying their error coverage, as well as the area, power consumption and delay overheads of encoder and decoder circuits.

This work is organized as follows. Section 2 summarizes the basic behaviour of the Matrix-based codes, including FUEC-M code. Section 3 introduces the characteristics of FUEC-ME. Section 4 presents the results of the evaluation of the different ECCs. Finally, Section 5 concludes this work.

2 Matrix-based Error Correction Codes

2.1 Introduction to Matrix-based Error Correction Codes

Traditionally, a Matrix-based ECC is an Error Correction Code that organizes the data in a two-dimensional form, in such a way that the combination of two, or more, ECCs allows to increase its detection and/or correction capabilities. In the specific case of adjacent errors, both horizontal and vertical dimensions must be considered [14], [15], [21], [22], [23].

An example is shown in Fig. 1 (extracted from [15]), where X_i represents the data bits, C_j and Pa_k are the horizontal control bits (calculated using an Extended Hamming SEC-DED code), and P_n are the vertical parity bits. This matrix code, called CLC, is able to correct all single errors, as well as different types of adjacent errors, as we will see in Section 4.

X_1	X_2	X_3	X_4	C_1	C_2	C_3	Pa_1
X_5	X_6	X_7	X_8	C_4	C_5	C_6	Pa_2
X_9	X_{10}	X_{11}	X_{12}	C_7	C_8	C_9	Pa_3
X_{13}	X_{14}	X_{15}	X_{16}	C_{10}	C_{11}	C_{12}	Pa_4
P_1	P_2	P_3	P_4	P_5	P_6	P_7	P_8

Fig. 1. Layout of CLC ECC [15].

CLC presents two great advantages. On the one hand, it improves the error coverage of Extended Hamming SEC-DED ECC or the parity checks. The combination of both ECCs allows to increase their detection and correction rate. CLC code is able to correct all single errors, as well as to correct or detect all 2-bit adjacent errors.

On the other hand, the overhead caused when using Hamming codes and parity bits is not very high, since encoders and decoders circuits are usually very efficient.

However, this ECC introduces a very high redundancy, which causes an increase in the memory required for the code bits. If we calculate the redundancy using expression (1), we can see that this code has a redundancy of *150%.* This high number provokes a reduction in the available memory for the payload.

$$Redundancy = \frac{No.\ code\ bits}{No.\ data\ bits} \times 100 \quad (1)$$

2.2 FUEC-M Error Correction Code

In a previous work, we presented FUEC-M [18], a two-dimensional code that improves the performance of the CLC [15]. With the scheme shown in Fig. 2 (where Xi represents the data bits and Cj the control bits calculated using the FUEC-M code), this new matrix code introduces a smaller number of redundant bits.

In particular, if we apply expression (1), redundancy of FUEC-M is *56.25%.* This low redundancy implies a greater memory availability to store data bits. For example, in the case of CLC [15], in a 1GB memory chip, only 410MB will be available to store data bits, since the remaining 614MB are needed to store the code bits. In the case of the FUEC-M [18], only 370MB are necessary to store the code bits, being the rest, about 655MB, used to store the data bits.

Another difference between the CLC and FUEC-M is their error coverage. Specifically, FUEC-M is able to correct single errors, adjacent double errors in both horizontal and vertical dimensions, and adjacent quadruple errors in 2x2 squares.

C_0	C_1	C_2	C_3	C_4
C_5	C_6	C_7	C_8	X_0
X_1	X_2	X_3	X_4	X_5
X_6	X_7	X_8	X_9	X_{10}
X_{11}	X_{12}	X_{13}	X_{14}	X_{15}

Fig. 2. Layout of FUEC-M ECC [18].

3 FUEC-ME Error Correction Code

In [30], we have presented a new ECC (called FUEC-ME) that extends the error correction features of FUEC-M using the same number of redundant bits. Specifically, this new code can correct single errors, adjacent double errors in both horizontal and vertical dimensions, and adjacent quadruple errors in 2x2 squares, as FUEC-M does. And, in addition, FUEC-ME can also correct 3-, 4- and 5-bit adjacent errors, both horizontally and vertically, and square errors of 3x2, 2x3 and 3x3 bits.

An ECC is defined by a parity check matrix **H** [8], [18]. In particular, the parity check matrix **H** that defines the FUEC-ME code can be seen in Fig. 3.

$$H = \begin{array}{c} \begin{matrix} C_0 C_1 \cdots\cdots C_8 X_0 \cdots\cdots\cdots\cdots X_{15} \end{matrix} \\ \left|\begin{matrix} 100000000110001001000000 \\ 010000000001100100000 1000 \\ 001000000100010000001 0001 \\ 000100000010000010010 0100 \\ 000010000001010000000011 \\ 000001000000100000101 0001 \\ 000000100000001000010 0101 \\ 000000010000000110110 0000 \\ 000000001000000001001 1010 \end{matrix}\right| \end{array}$$

Fig. 3. Parity check matrix **H** of FUEC-ME ECC [30].

From **H**, we can easily deduce the formulas to encode the data and for obtaining the syndrome bits, as it can be seen in Table 1. Specifically, Table 1-a shows the formulas to calculate the code bits that are stored with each data word, while Table 1-b shows the formulas to obtain the syndrome bits that will be used for the correction of errors.

Table 1. Formulas obtained from parity check matrix **H** of Fig. 3

$C_0 = X_0 \oplus X_1 \oplus X_5 \oplus X_8$	$s_0 = C_0 \oplus X_0 \oplus X_1 \oplus X_5 \oplus X_8$
$C_1 = X_2 \oplus X_3 \oplus X_6 \oplus X_{12}$	$s_1 = C_1 \oplus X_2 \oplus X_3 \oplus X_6 \oplus X_{12}$
$C_2 = X_0 \oplus X_4 \oplus X_{11} \oplus X_{15}$	$s_2 = C_2 \oplus X_0 \oplus X_4 \oplus X_{11} \oplus X_{15}$
$C_3 = X_1 \oplus X_7 \oplus X_{10} \oplus X_{13}$	$s_3 = C_3 \oplus X_1 \oplus X_7 \oplus X_{10} \oplus X_{13}$
$C_4 = X_2 \oplus X_4 \oplus X_{14} \oplus X_{15}$	$s_4 = C_4 \oplus X_2 \oplus X_4 \oplus X_{14} \oplus X_{15}$
$C_5 = X_3 \oplus X_9 \oplus X_{11} \oplus X_{15}$	$s_5 = C_5 \oplus X_3 \oplus X_9 \oplus X_{11} \oplus X_{15}$
$C_6 = X_5 \oplus X_{10} \oplus X_{13} \oplus X_{15}$	$s_6 = C_6 \oplus X_5 \oplus X_{10} \oplus X_{13} \oplus X_{15}$
$C_7 = X_6 \oplus X_7 \oplus X_9 \oplus X_{10}$	$s_7 = C_7 \oplus X_6 \oplus X_7 \oplus X_9 \oplus X_{10}$
$C_8 = X_8 \oplus X_{11} \oplus X_{12} \oplus X_{14}$	$s_8 = C_8 \oplus X_8 \oplus X_{11} \oplus X_{12} \oplus X_{14}$
a)	b)

4 Evaluation of Matrix-based Codes

In this section, we will introduce the error models commonly used in coding theory. Afterwards, we will present the results obtained during the evaluation of the different ECCs presented previously: CLC [15], FUEC-M [18] and FUEC-ME [30].

This evaluation has been carried out through two different processes. First, different types of errors have been injected into the C models of the ECCs under study. With this method, it is possible to evaluate their error coverage. In a second step, the different encoder and decoder circuits have been implemented in VHDL. In this way, we have been able to synthesize them in order to estimate the overheads introduced with respect to the area, power consumption and delay.

4.1 Error Models

The term *random error* is defined in coding theory as one or more erroneous bits, randomly distributed in a code word. This code word includes the data bits plus the code bits generated by the ECC.

Random errors can be *single* or *multiple*. *Single errors* affect a single memory cell. They are commonly produced by Single Event Upsets (SEU, in RAM) or Single Event Transients (SET, in combinational logic) [19]. On the other hand, *multiple errors* affect more than one memory cell, becoming more frequent due to technology scaling [3], [4], [5], [6], [7]. This type of error commonly appear grouped in neighbouring bits, rather than randomly. *Adjacent errors*, that is, multiple errors where all the erroneous bits are contiguous, can be generated when a cosmic particle hits a memory cell [19]. This is the most frequent type of multiple error [4], [20].

4.2 Error coverage evaluation

By using a simulation-based fault injector developed in a previous work [24], we have been able to study the error coverage of the ECCs presented in previous sections. The basic scheme of the injection tool is shown in Fig. 4.

Using this tool, we can inject different types of errors, being able to check if the final data word is correct or not. In addition, the tool can also generate the NRE (*Non Recoverable Error*) signal when an error is detected but it cannot be corrected. In this way, and by injecting all the errors of a given size and model, it is possible to count the number of errors corrected and/or detected with respect to the total number of possible errors. Thus, the error coverage of each code can be calculated.

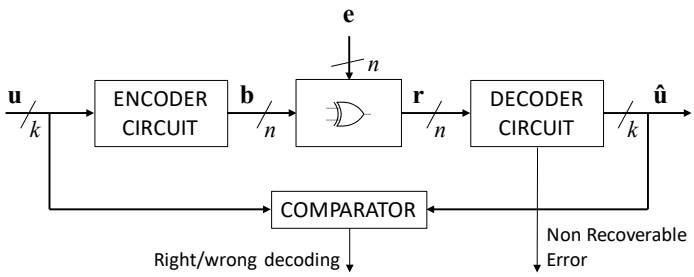

Fig. 4. Block diagram of the simulation-based fault injector tool [24].

We have not injected errors according to their probability of occurrence. Instead, we have injected each type of error (single or adjacent errors of different lengths) in all the bits of the code word. In this way, it has been possible to check the error correction capabilities of the different ECCs.

The different blocks of the fault injection tool of Fig. 4 have been implemented in C. Bit logic operators have been used in order to accurately simulate the hardware behaviour. From the parity check matrix **H**, the coding and decoding circuits of the different ECCs are easily obtained. These circuits are implemented in C through functions, so switching from one ECC to another is as simple as adjusting the word lengths and replacing the coding and decoding functions for the new ECC.

In this work, we have injected the same errors than [28], in order to accurately compare the behaviour of FUEC-ME code with respect to CLC and FUEC-M codes. With the data obtained in the different fault injection experiments, and using formula (2), we have calculated the error correction coverage of the different ECCs:

$$C_{correc} = \frac{Errors\_Corrected}{Errors\_Injected} \times 100 \qquad (\mathbf{2})$$

where $Errors\_Corrected$ are the number of errors corrected by the corresponding ECC, and $Errors\_Injected$ are the total amount of errors injected for a given error type.

Table 2 shows the results obtained. As expected, the new code FUEC-ME can correct all the errors we have injected: single errors, adjacent errors from 2- to 5-bit lengths, both horizontally and vertically, and different square patterns of adjacent errors, such as 2x2, 2x3, 3x2 and 3x3. As you can see, these results improve those obtained by the FUEC-M code [19], just as we had proposed when designing the FUEC-ME code.

In summary, FUEC-ME code allows the correction of different types of adjacent errors with a very low redundancy. If the behaviour of the memory to be protected is affected by this type of errors (adjacent errors with a length bigger than 2 bits and with different patterns), FUEC-ME code is a good alternative, for two main reasons: i) its low redundancy; and ii) its high error correction coverage.

Table 2. Error correction coverages

	CLC [15]	FUEC-M [18]	FUEC-ME [30]
Horizontal Error Pattern			
Error Length	% Corrected Errors	% Corrected Errors	% Corrected Errors
1	100,00	100,00	100,00
2	100,00	100,00	100,00
3	100,00	0,00	100,00
4	68,00	0,00	100,00
5	100,00	0,00	100,00
Vertical Error Pattern			
Error Length	% Corrected Errors	% Corrected Errors	% Corrected Errors
1	100,00	100,00	100,00
2	50,00	100,00	100,00
3	100,00	6,67	100,00
4	50,00	0,00	100,00
5	100,00	0,00	100,00
Square Error Pattern			
Error Length	% Corrected Errors	% Corrected Errors	% Corrected Errors
2x2	42,86	100,00	100,00
3x2	100,00	0,00	100,00
2x3	33,33	0,00	100,00
3x3	16,67	0,00	100,00

4.3 Synthesis results

We have seen in Section 3 that FUEC-ME code has the same redundancy as FUEC-M code, and a lower redundancy than CLC code. Also, we have verified in Section 4.2 that FUEC-ME code can correct a greater number and type of adjacent errors than FUEC-M and CLC codes.

In this section, we will study the overheads, with respect to silicon area, power consumption and delay, introduced by the FUEC-ME code. We will also compare them with the overheads introduced by CLC and FUEC-M codes. To do this, the different encoders and decoders circuits have been synthesized. In particular, these circuits have been implemented in VHDL. Then, and using CADENCE software [25], we have made a logical synthesis for 45 nm technology, through the use of the Nan-Gate FreePDK45 library [26], [27].

Fig. 5 shows the area overhead of the different encoder and decoder circuits. As it can be seen, FUEC-ME encoder introduces a similar overhead than FUEC-M encoder, and smaller than CLC encoder one's. In the case of the decoder, the biggest overhead corresponds to the FUEC-ME decoder. This is an expected result, as this ECC presents the highest error coverage, as seen in Table 2.

Fig. 6 shows the power consumption overhead. Consumption is directly related to the area occupied. In this way, encoder power overhead of FUEC-ME presents a

consumption slightly higher than the FUEC-M overhead, and lower than CLC one. In the case of the decoder, FUEC-ME presents the highest overhead, as this ECC has introduced the largest area.

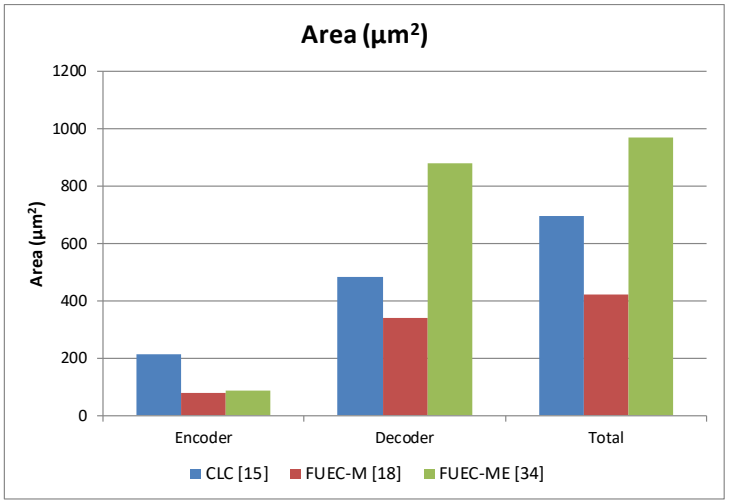

Fig. 5. Area overheads.

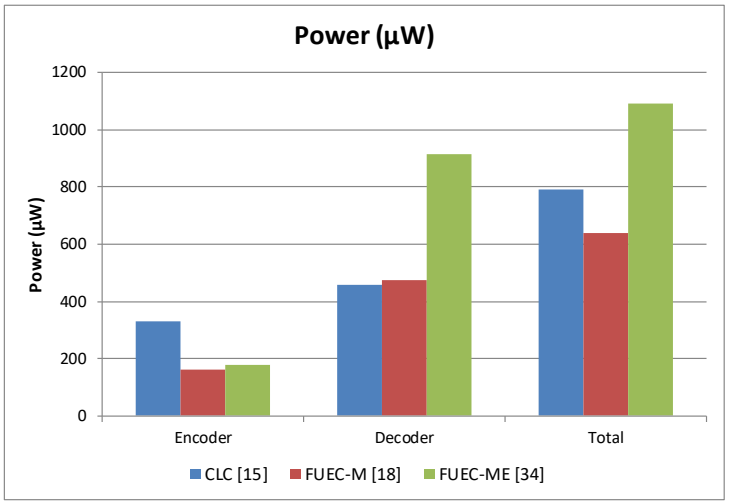

Fig. 6. Power overhead.

Finally, Fig. 7 shows the delay overhead. As with the area and power consumed, the greater error coverage of FUEC-ME code causes a higher delay. This fact can be clearly seen in the case of the decoder. In order to obtain its high error coverage, the number of operations to be performed by FUEC-ME code causes a greater delay.

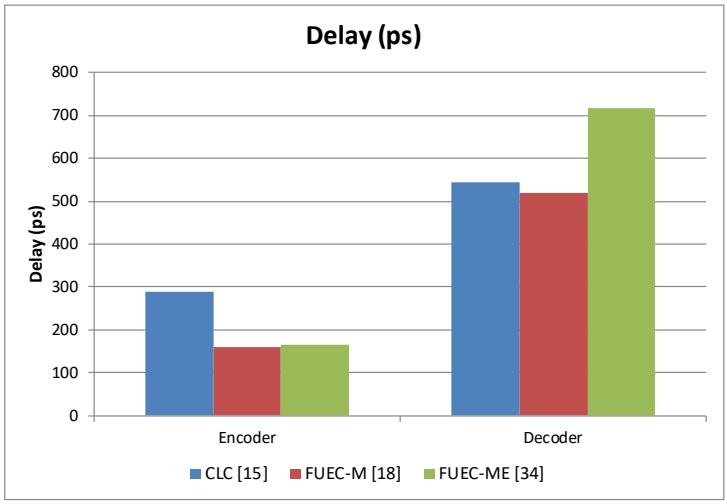

Fig. 7. Delay overhead.

We can conclude that FUEC-ME code presents a higher overhead than CLC and FUEC-M codes, mainly in the decoder. This greater overhead is provoked by, on the one hand, the low number of redundant bits of FUEC-ME code, and, on the other hand, the greater error coverage of this code.

5 Conclusions

In this work, we have presented a comparison between different Matrix-based Error Correction Codes. In this way, we have verified the efficiency of the different ECCs by comparing both the error correction coverages and the overheads introduced in the silicon area, power consumption and delay.

With respect to the error correction coverage, new FUEC-ME code greatly exceeds the error correction coverage of the compared ECCs. Specifically, FUEC-ME code can correct 100% of single errors, as well as 100% of adjacent errors of length from 2- to 5-bits, both horizontally and vertically. Also, adjacent errors with different square patterns, such as 2x2, 2x3, 3x2 and 3x3, can be tolerated.

On the other hand, FUEC-ME code introduces a greater overhead with respect to area, power and delay, mainly due to its greater error coverage.

In general, FUEC-ME code complements FUEC-M code, being the latter ECC an appropriate option for applications where double adjacent errors are expected, while FUEC-ME code can be used in those applications in which adjacent errors of larger size are expected.

In future works, we want to continue developing low redundant ECCs trying also to reduce the overheads in area, power and delay, maintaining, or even improving, the error coverage. On the other hand, we also want to develop other ECCs focused on

larger adjacent multiple errors, which are expected to have an increasingly important impact.

References

1. The International Technology Roadmap for Semiconductors 2013. [Online]. Available at: http://www.itrs2.net/2013-itrs.html
2. S.K. Kurinec and K. Iniewsky. Nanoscale Semiconductor Memories: Technology and Application, CRC Press, Taylor & Francis Group, 2014.
3. E. Ibe, H. Taniguchi, Y. Yahagi, K. Shimbo, and T. Toba, "Impact of scaling on neutron-induced soft error in SRAMs from a 250 nm to a 22 nm design rule", IEEE Trans. Electron Devices, vol. 57, no. 7, pp. 1527–1538, July 2010.
4. G. Tsiligiannis et. al., "Multiple Cell Upset Classification in Commercial SRAMs", IEEE Transactions on Nuclear Science, vol. 61, no. 4, August 2014.
5. G.I. Zebrev, "Multiple Cell Upset Cross-Section Uncertainty in Nanoscale Memories: Microdosimetric Approach", 15th European Conference on Radiation and its Effects on Components and Systems (RADECS 2015), September 2015.
6. N.G. Chechenin and M. Sajid, "Multiple cell upsets rate estimation for 65 nm SRAM bit-cell in space radiation environment", 3rd International Conference and Exhibition on Satellite & Space Missions, May 2017.
7. N.N. Mahatme, B.L. Bhuva, Y.P. Fang, and A.S. Oates, "Impact of strained-Si PMOS transistors on SRAM soft error rates", IEEE Trans. on Nuclear Science, vol. 59, no. 4, pp. 845–850, August 2012.
8. E. Fujiwara, Code Design for Dependable Systems: Theory and Practical Application, Ed. Wiley-Interscience, 2006.
9. R. W. Hamming, "Error detecting and error correcting codes," Bell System Technical Journal, vol. 29, pp. 147–160, 1950.
10. C.L. Chen and M.Y. Hsiao, "Error-correcting codes for semiconductor memory applications: a state-of-the-art review", IBM Journal of Research and Development, vol. 58, no. 2, pp. 124–134, March 1984.
11. G.C. Cardarilli, M. Ottavi, S. Pontarelli, M. Re, and A. Salsano, "Fault Tolerant Solid State Mass Memory for Space Applications", IEEE Trans. on Aerospace and Electronic Systems, vol. 41, no. 4, pp. 1353–1372, October 2005.
12. S. Pontarelli, G.C. Cardarilli, M. Re and A. Salsano, "Error correction codes for SEU and SEFI tolerant memory systems", 24th IEEE International Symposium on Defect and Fault Tolerance in VLSI Systems (DFT 2009), pp. 425-430, 2009.
13. A. Sánchez-Macián, P. Reviriego, J. Tabero, A. Regadío, and J.A. Maestro, "SEFI protection for Nanosat 16-bit Chip On-Board Computer Memories", IEEE Transactions on Device and Materials Reliability, DOI 10.1109/TDMR.2017.2750718, 2017.
14. C. Argyrides, D.K. Pradhan, and T. Kocak, "Matrix codes for reliable and cost efficient memory chips", IEEE Transactions on Very Large Scale Integration (VLSI) Systems, vol. 19, nº 3, pp.420–428, March 2011.
15. H.S. de Castro, et al. "A correction code for multiple cells upsets in memory devices for space applications", 2016 14th IEEE International New Circuits and Systems Conference (NEWCAS 2016), pp.1–4, June 2016.
16. S. Ahmad, M. Zahra. S.Z. Farooq, and A. Zafar, "Comparison of EDAC schemes for DDR memory in space applications", 2013 International Conference on Aerospace Science & Engineering (ICASE 2013), August 2013.
17. D.E. Muller, "Application of boolean algebra to switching circuit design and to error detection", IRE Transactions on Electronic Computers, vol. 3, pp. 6–12, 1954.

18. J. Gracia-Morán, L.J. Saiz-Adalid, D. Gil-Tomás, P.J. Gil-Vicente, "Un nuevo Código de Corrección de Errores matricial con baja redundancia", III Jornadas de Computación Empotrada y Reconfigurable (JCER2018), Jornadas SARTECO, pp. 561-566, September 2018.
19. M. Murat, A. Akkerman, and J. Barak, "Electron and ion tracks in silicon: Spatial and temporal evolution," IEEE Transactions on Nuclear Science, vol. 55, no. 6, pp. 3046–3054, December 2008.
20. M. Wirthlin, D. Lee, G. Swift, and H. Quinn, "A method and case study on identifying physically adjacent multiple-cell upsets using 28-nm, interleaved and SECDED-protected arrays," IEEE Transactions on Nuclear Science, vol. 61, no. 6, pp. 3080–3087, Dec. 2014.
21. S. Liu, L. Xiao, J. Li, Y. Zhou, and Z. Mao, "Low Redundancy Matrix-Based codes for Adjacent Error Correction with Parity Sharing", 2017 18th International Symposium on Quality Electronic Design (ISQED 2017), March 2017.
22. P. Reviriego and J.A. Maestro, "Efficient Error Detection Codes for Multiple-Bit Upset Correction in SRAMs with BICS", ACM Transactions on Design Automation of Electronic Systems (TODAES) Vol. 14 nº 1, January 2009.
23. M. Zhu, L. Xiao, S. Li, and Y. Zhang, "Efficient Two-Dimensional Error Codes for Multiple Bit Upsets Mitigation in Memory", 2010 25th International Symposium on Defect and Fault Tolerance in VLSI Systems (DFT 2010), pp. 129-135, October 2010.
24. J. Gracia-Moran, L.J. Saiz-Adalid, D. Gil-Tomás, and P.J. Gil-Vicente, "Improving Error Correction Codes for Multiple Cell Upsets in Space Applications", IEEE Transactions on Very Large Scale Integration (VLSI) Systems, vol. 26(10), pp. 2132-2142, October 2018.
25. *Cadence: EDA Tools and IP for System Design Enablement*. [Online]. Available at: https://www.cadence.com/
26. J.E Stine et al., "FreePDK: An Open-Source Variation-Aware Design Kit", IEEE International Conference on Microelectronic Systems Education (MSE'07), June 2007.
27. *NanGate FreePDK45 Open Cell Library*. [Online]. Available at: https://www.eda.ncsu.edu/wiki/FreePDK45:Contents
28. J. Gracia-Morán, L.J. Saiz-Adalid, D. Gil-Tomás, P.J. Gil-Vicente, "A comparison of two different matrix Error Correction Codes", Workshop on Innovation on Information and Communication Technologies (ITACA-WIICT 2018), pp. 74-83, July 2018.
29. J. Gracia-Morán, L.J. Saiz-Adalid, J.C. Baraza-Calvo, P.J. Gil-Vicente, "Correction of Adjacent Errors with Low Redundant Matrix Error Correction Codes", 8th Latin-American Symposium on Dependable Computing (LADC 2018), pp. 107-114, October 2018.
30. J. Gracia-Morán, L.J. Saiz-Adalid, D. Gil-Tomás, J.C. Baraza-Calvo, P.J. Gil-Vicente, "Mejora de un Código de Corrección de Errores para tolerar fallos adyacentes bidimensionales", submitted to IV Jornadas de Computación Empotrada y Reconfigurable (JCER2018), Jornadas SARTECO, September 2019.

Division of the Left Ventricle in AHA Segments. A Criteria Comparison applied to Radial Strain.

Yolanda Vives-Gilabert, José Millet,Francisco Castells

Instituto ITACA, Universitat Politècnica de València, Spain

Abstract. The 17-segments model defines 6 segments in the basal and mid-cavity levels, 4 in the apical level and the apex. In the basal and mid-cavity levels, the standard recommends the division in 6 equiangular segments beginning from a right ventricle insertion point, but many studies take both insertion points getting 6 non-equiangular segments. The aim of this study is to compare the influence of two segmentation criteria in terms of wall thickness and strain and how it affects to different pathologies. 80 subjects from the ACDC dataset were used. The area of different segments changed significantly as a function of the segmentation criteria. In terms of pathology, only the subtraction of the two criteria in the angle S10-11 were statistically significant. Mean wall thickness and radial peak strain values were similar, but some subjects presented important differences between models, which could lead to errors if individual values were considered.

1 Introduction

Characterization of the left ventricle of the heart in anatomical segments convey clinical importance. The American Heart Association (AHA) suggested in 2002 a division of the left ventricle for tomographic imaging into 17 segments, where the left ventricle (LV) was divided longitudinally in 3 sections (basal, mid and apical) and radially in 4 or 6 segments [1]. This model has been widely used in cardiac magnetic resonance (CMR), providing a successful harmonization, however, the definition of how some segments are partitioned deserves further clarification. The AHA guidelines state that, for the basal and mid-cavity slices, the LV should be divided into 6 equiangular segments starting from the right ventricular (RV) insertion point, but as it is not clear which insertion point to use, many manuscripts use both to delineate the septum, which results in 6 non-equiangular segments [2].

In a recent report, Selvadurai et al. tried to clarify this aspect by recommending the use of both RV insertion points to define two major axes that divide the heart in four segments, and for the basal and mid-cavity levels, the septal and the lateral area would be further divided using an equiangular line to generate 6 segments [3]. This definition avoids possible misalignments of segments either at the anterior or at the inferior RV insertion points, however, the size of the lateral segments is subjected to the size of the septum.

C.Fernandez-Llatas and M.Guillen (Ed.):
Workshop on Innovation on
Information and Communication Technologies
(ITACA-WIICT 2019)

ISBN 978-84-09-17526-0

The differences in size of the different segments can affect the characterization of the LV in terms of localized quantitative measures like the wall thickness or the strain, which are features of many cardiac diseases. For example, hypertrophic cardiomyopathy is defined by increased LV wall thickness ($\geq 15mm$) in one or more LV myocardial segments [4] and dilated cardiomyopathy is characterized by segmental wall motion abnormalities [5].

The aim of this paper is to study the influence of two different criteria in the definition of the AHA segments when they are applied to CMRs of patients with different pathologies like dilated cardiomyopathy, hypertrophic cardiomyopathy, myocardial infarction and to healthy subjects.

2 Materials and Methods

2.1 Sample

The sample comprises 80 subjects from the training set of ACDC (Automated Cardiac Diagnosis Challenge) dataset, from the MICCAI challenge 2017 [6]. This subset is composed of 20 subjects with DCM (dilated cardiomyopathy), 20 with HCM (hypertrophic cardiomyopathy), 20 with MINF (myocardial infarction) and 20 NOR (normal subjects). The characterization of these groups and the details regarding the data acquisition can be found in Bernard et al. [6].

For each subject, we used the end-systole and the end-diastole 3D CMRs, with their respective ground truth segmentations as provided by the dataset. Both RV and LV segmentations were used in the analysis.

2.2 AHA Segmentation

According to the standardized myocardial segmentation of the American Heart Association, the LV can be divided longitudinally in 3 sections (basal, mid-cavity and apical) and cross-sectionally into 17 segments, with 6 segments in the basal and mid-cavity levels, 4 segments in the apical level and the 17^{th} segment at the bottom of the LV (apex) (Fig. 1). As the dataset does not contain a complete true apex, only segments 1 to 16 were evaluated in this study.

For the segmentation of the LV in 16 segments, we used both anterior and inferior RV insertion points [3]. The septal and lateral area were divided with an equiangular line. For the rest of the segments, two criteria were applied, as illustrated in Fig. 1:

- Method 1 (M1): the RV insertion points were used to define 2 major axes.
- Method 2 (M2): the RV insertion points defined the anteroseptal and the inferoseptal segments. The rest of the area was divided in 4 equiangular segments.

We assume that both LV and RV were obtained previously with an automatic or a manual segmentation method. The RV insertion points were detected by obtaining a boundary line between RV and LV and taking the minimum and

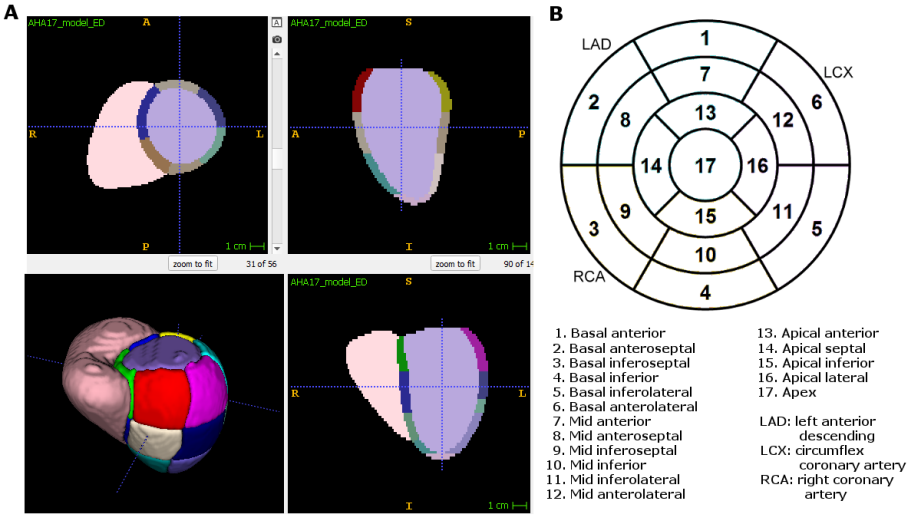

Fig. 1. Atlas with the localization of the 17 segments (A) and bull's eye display (B)

the maximum points in polar coordinates. The longitudinal division of the LV in basal, mid-cavity and apical sections was done equitably.

The angle subtraction between M1 and M2 was calculated for angles S1-S6 (angle between segment 1 and segment 6) and S4-S5 (angle between segment 4 and segment 5) in the basal level and S7-S12 (angle between segment 7 and segment 12) and S10-S11 (angle between segment 10 and segment 11) in the mid-cavity level (Fig. 2). All the calculations were performed with MATLAB and Image Processing Toolbox Release 2016a, The MathWorks, Inc., Natick, Massachusetts, United States.

Afterwards we studied the possible relationship between the angle differences and the pathology of the patients. For that purpose, we performed a one-way ANOVA and a Bonferroni post-hoc analysis with $p = 0.05$. The statistical tests were carried out with IBM SPSS (version 23, SPSS Statistics/IBM Corp, Chicago II, USA). Boxplots were represented in Matlab.

2.3 Wall-thickness and Strain

Wall-thickness was measured by calculating the minimum Euclidean distance between the endocardium and the epicardium at each point of the endocardium. Afterwards, the mean value of each segment was obtained.

Myocardial strain is defined as the deformation of the myocardial in one of three different directions: radial, circumferential or longitudinal. Radial strain gives a measure of the relationship between the wall thickening during the systole and the wall thinning during the diastole, circumferential strain shows the fiber shortening along the circular perimeter and the longitudinal strain derives from

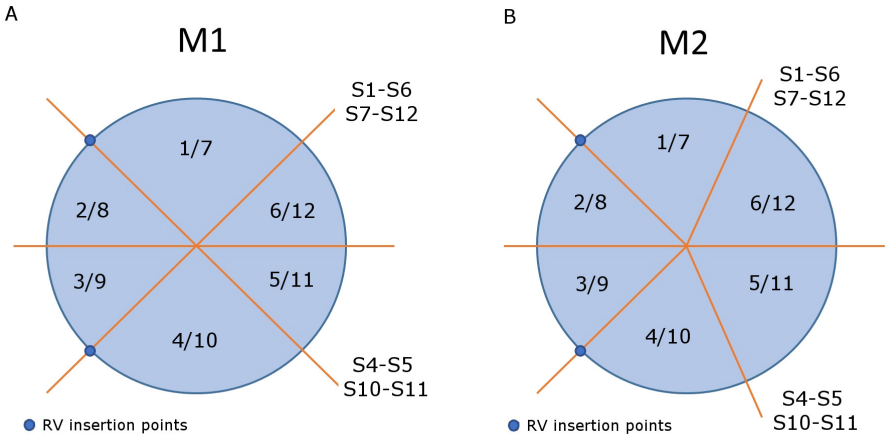

Fig. 2. Segmentation criteria in the basal/mid-cavity levels: method 1 (A) and method 2 (B)

the longitudinal shortening from the base to the apex. Strain values can be global or local (strain per segments) values.

In this work, we calculated the maximum radial strain values for each subject and each segment. For this purpose, we obtained the wall thickness at end-diastole and at end-systole in all the 16 AHA segments. The peak radial strain (PRS) was calculated according to equation 1:

$$PRS = \frac{WT(s) - WT(d)}{WT(d)} \tag{1}$$

with WT(s) the wall-thickness at end-systole and WT(d) the wall-thickness at end-diastole.

Then we compared the results of wall-thickness and peak radial strain obtained with method 1 (M1) and with method 2 (M2) by subtracting M1 results to M2 results and taking the absolute value. All these calculations were also performed with MATLAB.

Finally, to study if the differences of segmentation criteria could lead to different statistical results according to the pathology, an M1 and an M2 one-way ANOVAs between the four groups were performed.

3 Results

We present in Fig. 3 an example of a subject (DCM, basal (upper row) and mid-cavity (down row) levels at end-diastole) segmented with method 1 (M1) and method 2 (M2).

While segments 2, 3, 8 and 9 remain identical in both methods, the area covering segments 1,4, 5 and 6 changes a little bit, and 7, 10, 11 and 12 change

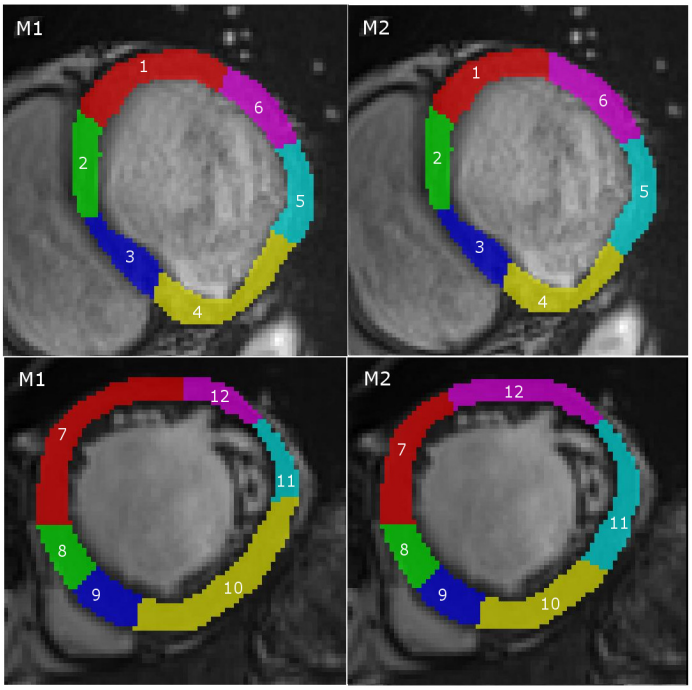

Fig. 3. CMR AHA segmentation applying method 1 (M1) and method 2 (M2) in the basal level (upper row) and in the mid-cavity level (down row)

significantly. These differences depend on the length of the septal wall and are more remarkable in the mid-cavity level than in the basal level.

When we analyzed the angle subtraction as a function of the pathology, we found significant differences between groups in angle S10-S11 at end-systole, $F(3, 76) = 11.7, p < 0.001$, and at end-diastole, $F(3, 76) = 6.6, p = 0.001$, while the other angles did not reach statistical differences (Fig. 4).

Post-hoc analyses revealed significant differences between HCM and DCM (end-systole $p < 0.001$, end systole $p = 0.04$) and between HCM and NOR (end-systole $p < 0.001$, end-diastole $p < 0.001$). HCM and MINF presented significant differences ($p < 0.006$) only at end-systole.

3.1 Wall-thickness and Strain

The differences of wall-thickness and peak radial strain between segmentation method 1 and segmentation method 2 were small (Table 1). Segments 10 and 11 of the mid-cavity level presented the higher differences in terms of wall thickness and radial strain.

However, in general standard deviations were high, which indicates that some patients presented important differences when segments were obtained with M1

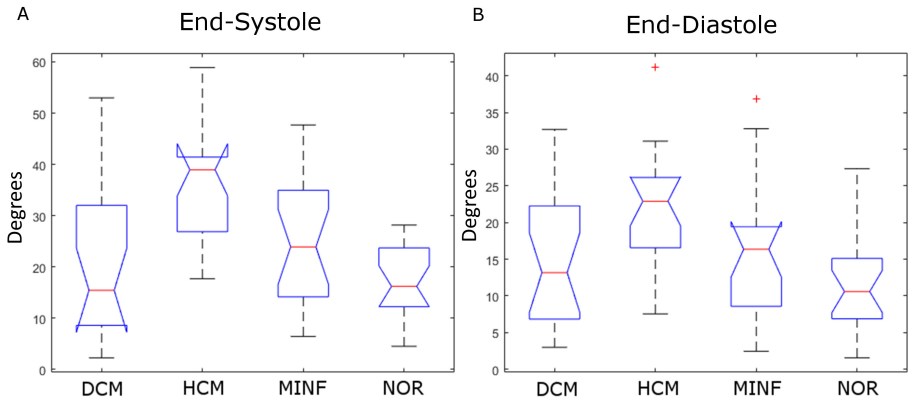

Fig. 4. $|M1(S10 - S11) - M2(S10 - S11)|$ at end-systole (A) and end diastole (B)

or with M2, especially in strain. Table 2 shows some examples of subjects with important differences between M1 and M2 in peak radial strain for segment 10.

The two one-way ANOVA group analyses (one with data extracted applying M1 and the second with data obtained applying M2) revealed the same results: significant differences in all the segments and similar mean values in each group.

4 Discussion and Conclusions

In this study we compared two criteria to segment the LV in 16 AHA segments (the 17^{th} segment was not taken into consideration). The first method, already applied in many papers, follows the recommendation of Selvadurai et al.[3], where the division is based on two major axes defined by both RV insertion points. The second method also defines the septal segments with both RV insertion points, but the rest of the LV is divided in 4 equiangular segments. This method is an attempt to fuse method 1 and the original AHA guidelines, that advocates the divison of the LV into 6 60-degree segments starting from a RV insertion point.

The main difference between M1 and M2 lies in the septal length. If this length is higher, as in the basal slices, the differences between both methods are smaller than in the mid-cavity, where the RV is smaller and the septal length too. In this case, the application of M1 is translated into smaller septal and lateral segments, while anterior and inferior segments are bigger. With M2, even is septal segments continue being smaller, the rest of the segments are equal.

The major angle differences of segmenting the LVs using M1 or M2 criteria were found in the HCM group of patients, with significant differences between DCM and NOR groups in the angle S10-S11 in both end-systole and end-diastole (Fig. 4). With this test we showed that according to the physiology of the LV in some cases altered by a determinate pathology, segmenting with one or other criteria can vary the angles significantly.

Table 1. Mean differences of wall thickness at end-systole, end-diastole and radial strain between M1 and M2 for each segment calculated as $|M1 - M2|$

Segment	Wall-thickness end-systole (mm)	Wall-thickness end-diastole (mm)	Radial Strain
1	0.09 ± 0.14	0.15 ± 0.19	3.30 ± 4.09
4	0.10 ± 0.12	0.15 ± 0.15	3.08 ± 2.96
5	0.15 ± 0.25	0.22 ± 0.24	3.72 ± 3.67
6	0.09 ± 0.14	0.18 ± 0.19	3.03 ± 2.93
9	0.08 ± 0.08	0.16 ± 0.51	2.48 ± 2.51
10	0.13 ± 0.15	0.27 ± 0.32	4.54 ± 4.78
11	0.17 ± 0.23	0.36 ± 0.50	5.07 ± 8.67
12	0.08 ± 0.09	0.15 ± 0.15	2.85 ± 3.29
13	0.12 ± 0.21	0.20 ± 0.26	4.85 ± 5.60
14	0.13 ± 0.15	0.26 ± 0.31	4.41 ± 4.59
15	0.08 ± 0.11	0.14 ± 0.37	3.68 ± 5.29
16	0.12 ± 0.16	0.17 ± 0.22	5.07 ± 5.48

Table 2. Example of radial strain values of segment 10 obtained with M1 and M2

Group	Peak Radial Strain M1 (%)	Peak Radial Strain M2 (%)
Subject 2 (DCM)	37.34	84.64
Subject 36 (HCM)	79.03	84.64
Subject 51 (MINF)	15.88	29.97
Subject 68 (NOR)	63.2	53.29

Mean wall thickness and mean peak radial strain values were very similar when segmenting with M1 and M2. Consequently, group analyses of M1 and M2 led to similar results. However, as stated by the standard deviation of peak radial strain values from Table 1, some subjects presented high differences between both methods, as can be seen in the examples of Table 2. If peak radial strain values are taken into account individually, the segmentation method plays an important role in the calculation of these values. The differences in peak radial strain could also make that the peak value of strain is obtained in a different time phase of the cycle. This effect would cause an error in the calculation of the dyssynchrony [7], which is defined as the standard deviation of the time to peak strain.

From this study we can conclude that the effects of the segmentation criteria are reduced when performing group analysis because the differences are averaged. However, when individual values are considered, as for example to be compared with a determinate threshold, the segmentation criteria can be determinant. Defining the best segmentation criteria would request further analysis.

5 References

References

1. American Heart Association Writing Group on Myocardial Segmentation and Registration for Cardiac Imaging:, Cerqueira, M.D., Weissman, N.J., Dilsizian, V., Jacobs, A.K., Kaul, S., Laskey, W.K., Pennell, D.J., Rumberger, J.A., Ryan, T., Verani, M.S.: Standardized Myocardial Segmentation and Nomenclature for Tomographic Imaging of the Heart: A Statement for Healthcare Professionals From the Cardiac Imaging Committee of the Council on Clinical Cardiology of the American Heart Association. Circulation. 105, 539542 (2002).
2. Liang, X., Garnavi, R., Wail, S., Sisi Liang, null, Prasanna, P.: Automatic segmentation of the left ventricle into 17 anatomical regions in cardiac MR imaging. Conf Proc IEEE Eng Med Biol Soc. 2015, 65316535 (2015).
3. Selvadurai, B.S.N., Puntmann, V.O., Bluemke, D.A., Ferrari, V.A., Friedrich, M.G., Kramer, C.M., Kwong, R.Y., Lombardi, M., Prasad, S.K., Rademakers, F.E., Young, A.A., Kim, R.J., Nagel, E.: Definition of Left Ventricular Segments for Cardiac Magnetic Resonance Imaging. JACC: Cardiovascular Imaging. 11, 926928 (2018).
4. Authors Task Force members, Elliott, P.M., Anastasakis, A., Borger, M.A., Borggrefe, M., Cecchi, F., Charron, P., Hagege, A.A., Lafont, A., Limongelli, G., Mahrholdt, H., McKenna, W.J., Mogensen, J., Nihoyannopoulos, P., Nistri, S., Pieper, P.G., Pieske, B., Rapezzi, C., Rutten, F.H., Tillmanns, C., Watkins, H., Additional Contributor, OMahony, C., ESC Committee for Practice Guidelines (CPG), Zamorano, J.L., Achenbach, S., Baumgartner, H., Bax, J.J., Bueno, H., Dean, V., Deaton, C., Erol, ., Fagard, R., Ferrari, R., Hasdai, D., Hoes, A.W., Kirchhof, P., Knuuti, J., Kolh, P., Lancellotti, P., Linhart, A., Nihoyannopoulos, P., Piepoli, M.F., Ponikowski, P., Sirnes, P.A., Tamargo, J.L., Tendera, M., Torbicki, A., Wijns, W., Windecker, S., Document Reviewers, Hasdai, D., Ponikowski, P., Achenbach, S., Alfonso, F., Basso, C., Cardim, N.M., Gimeno, J.R., Heymans, S., Holm, P.J., Keren, A., Kirchhof, P., Kolh, P., Lionis, C., Muneretto, C., Priori, S.,

Salvador, M.J., Wolpert, C., Zamorano, J.L., Frick, M., Aliyev, F., Komissarova, S., Mairesse, G., Smaji, E., Velchev, V., Antoniades, L., Linhart, A., Bundgaard, H., Heli, T., Leenhardt, A., Katus, H.A., Efthymiadis, G., Sepp, R., Thor Gunnarsson, G., Carasso, S., Kerimkulova, A., Kamzola, G., Skouri, H., Eldirsi, G., Kavoliuniene, A., Felice, T., Michels, M., Hermann Haugaa, K., Lenarczyk, R., Brito, D., Apetrei, E., Bokheria, L., Lovic, D., Hatala, R., Garcia Pava, P., Eriksson, M., Noble, S., Srbinovska, E., zdemir, M., Nesukay, E., Sekhri, N.: 2014 ESC Guidelines on diagnosis and management of hypertrophic cardiomyopathy: The Task Force for the Diagnosis and Management of Hypertrophic Cardiomyopathy of the European Society of Cardiology (ESC). European Heart Journal. 35, 27332779 (2014).

5. Wallis, D.E., OConnell, J.B., Henkin, R.E., Costanzo-Nordin, M.R., Scanlon, P.J.: Segmental wall motion abnormalities in dilated cardiomyopathy: A common finding and good prognostic sign. Journal of the American College of Cardiology. 4, 674679 (1984).
6. Bernard, O., Lalande, A., Zotti, C., Cervenansky, F., Yang, X., Heng, P.-A., Cetin, I., Lekadir, K., Camara, O., Gonzalez Ballester, M.A., Sanroma, G., Napel, S., Pe-tersen, S., Tziritas, G., Grinias, E., Khened, M., Kollerathu, V.A., Krishnamurthi, G., Rohe, M.-M., Pennec, X., Sermesant, M., Isensee, F., Jager, P., Maier-Hein, K.H., Full, P.M., Wolf, I., Engelhardt, S., Baumgartner, C.F., Koch, L.M., Wolterink, J.M., Isgum, I., Jang, Y., Hong, Y., Patravali, J., Jain, S., Humbert, O., Jodoin, P.-M.: Deep Learning Techniques for Automatic MRI Cardiac Multi-Structures Segmen-tation and Diagnosis: Is the Problem Solved? IEEE Transactions on Medical Im-aging. 37, 25142525 (2018).
7. Vives-Gilabert, Y., Sanz-Sánchez, J., Molina, P., Cebrián, A., Igual, B., Calvillo-Batllés, P., Domingo, D., Millet, J., Martínez-Dolz, L., Castells, F., Zorio, E.: Left ventricular myocardial dysfunction in arrhythmogenic cardiomyopathy with left ventricular involvement: A door to improving diagnosis. International Journal of Cardiology. (2018).

The Research Career: a Systemic Approach

Jose Dahoui[1], Carles Boronat-Moll[2], Miguel-Ángel Hernández-García[3], and Jose-Luis Hervas-Oliver[2]

[1] Institute of Information and Communication Technologies, Universitat Politècnica de València, Valencia, 46022, Spain
jodaob@itaca.upv.es
[2] Management Department, Universitat Politècnica de València, Valencia, 46022, Spain
{carbomol, jose.hervas}@omp.upv.es
[3] Research & Innovation Office, Universitat Politècnica de València, Valencia, 46022, Spain
mhgarcia@upv.es

Abstract. The great challenge facing research structures is to improve the quantity and quality of their research practices, in order to achieve and maintain scientific excellence, which gives them greater visibility and increases access to external resources. Within these structures, groups, areas, laboratories and researchers, whose research practices and interests may be very different, can coexist. This heterogeneity is to blame for the fact that general policies to stimulate research activities of the structure may not adequately reach some of its members. This paper presents empirical evidence showing that a systemic approach, analyzing the research structure as a system, including its subsystems and their components, can help when designing more effective scientific production stimulus policies specifically addressed to certain of its elements. We measure the research activities of a research structure, which is part of a Spanish public university, its research groups and its researchers. The data analysis allows us to define the research practices profiles of the research groups and establish the orientation that stimulus policies aimed at each of them should have, validating our approach.

1 Introduction

Achieving high quality research practices not only provides greater visibility of a research structure, but also facilitates obtaining resources from external organizations, either through technical works done for third parties, intellectual property rights' licenses, or by obtaining projects funded by research grants. These resources facilitate the consolidation of the research structure as an excellent entity, as well as allow its growth.

Only those entities whose research practices reach very high levels of quality achieve excellence in research [1]. There are tools to measure the research excellence of a country [2], [3] or a higher education institution [4], [5], mainly based on establishing a system of performance indicators [6], [7]. Regarding units

C.Fernandez-Llatas and M.Guillen (Ed.):
Workshop on Innovation on
Information and Communication Technologies
(ITACA-WIICT 2019)

ISBN 978-84-09-17526-0

based at research institutions, some countries have distinctions as "Centers of Excellence in Research" (CoE) [8] - [10], although there is no universally extended scale for accessing this condition. In the particular case of Spain, Severo Ochoa Centres of Excellence and María de Maeztu Units of Excellence [11] set among their conditions a very high percentage of scientific publications in high impact journals within their respective thematic areas and a number of active doctors whose scientific publications have a standardized impact at least 50% higher than the world average value in their respective areas of specialization.

The quality of the research practices of a research structure depends on the excellence achieved by its parts, be they research groups, laboratories, areas, or any other forms of internal organization, and ultimately on the excellence achieved by its researchers.

The development of a person's research career and the consolidation of a research group are greatly affected by the environment, which in recent years has not been particularly favorable [12]. This environment sometimes places barriers to access financing that are not easily assumed without additional support.

However, the objectives, organization and research profiles of these parts may be different, so when defining policies that help improve the research performance of a structure, the policies may fall short for certain groups.

Understanding how different research groups and researchers work can lead to the design of more effective policies for certain groups or even be more efficient by targeting policies on those elements that have more room for improvement, taking into account that resources are limited. This paper aims to demonstrate that a systemic approach to these research structures and their subsystems and components can help us achieve this knowledge.

Each system and subsystem has its own structure and purpose. A system may be more than the sum of its parts if these different structures and purposes are harmonized, expressing synergy.

We will define a systemic model of the research structures and we will particularize it to a specific example in Section 2. We will define some performance indicators to analyse the subsystems of the specific example and demonstrate that these subsystems require different measures to improve their research results in Sections 3 and 4.

2 The system under study: the research structure

According to systems theory [13], [14], if our system under study is the research structure, research groups, laboratories or areas would be the most common subsystems or components thereof, which in turn could be broken down into other elements that would be the researchers, as well as other support staff (technicians, innovation managers, etc.). Typically, researchers are grouped into these subsystems, but it may be the case that there are some researchers not grouped in a research structure, especially in those research domains such as Mathematics or Social Sciences, where access to specialized resources like a laboratory is not necessary to carry out the research.

There is usually at least one research support unit within the research structure. When there are more than one, these units are usually specialized in specific tasks, such as attracting external funds, management of resources and protecting intellectual property rights.

All these subsystems usually have relationships between them. This does not imply that each subsystem necessarily has relations with all other subsystems. A general outline of the proposed model can be seen in Figure 1.

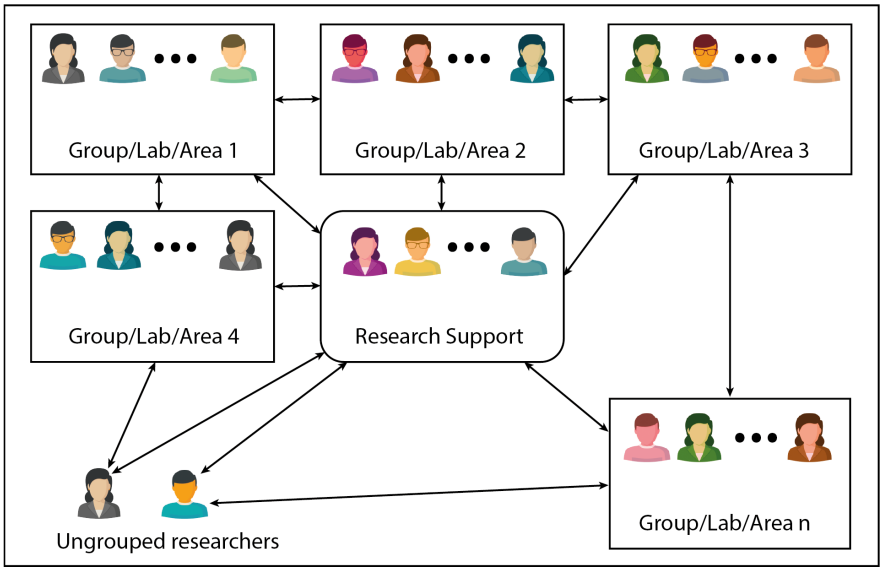

Fig. 1. Research structure model

These research structures, such as institutes and research centres, can in turn be part of other larger entities such as Universities, National Research Councils or Ministries. According to systems theory, these bigger organizations would act as suprasystems. In fact, a research structure could be part of two or more suprasystems. That is the case of the Joint Research Centers created by Universities and National Research Councils.

Within the suprasystem itself, the research structure may establish relationships with other research structures, especially those with complementary knowledge, or with other research support units generated by the suprasystem to support its components.

These systems are not invariable in time. For example, some excellent researchers will retire. Second level researchers should be prepared to take up the torch when the heads of the research groups leave the institution. Some research topics will no longer be a trend, so research groups will have to adapt their research to attractive topics for funders or give way to emerging groups. Some

researchers will progress in their research career, and create and lead their own research groups.

Not taking these potential changes into account and preparing the future can lead to losing the condition of excellent.

By definition [15], to be excellent you need to be outstanding. So research structures are dynamic systems trying to reach and maintain excellence, a concept that is not static, as it depends of the performance of other systems.

2.1 The particular case of ITACA Institute

The Institute of Information and Communication Technologies (ITACA) is a research structure of the Universitat Politècnica de València (UPV) that has the recognition of a University Research Institute since 2005, the highest research grade for research structures of Spanish Universities.

Although the UPV is a relatively young university, since it has just turned 50 years old, it has demonstrated a clear vocation for research and innovation [16]. In fact, its first research institutes, including ITACA, were founded in 1999 by UPV's Governing Board.

With more than twenty years of life, ITACA conducts research over a broad spectrum of different disciplines related to ICT. Since its origin, the ITACA Institute has had a very clear orientation towards ICT applications, which has made it one of the most successful UPV's research structures in raising funds from public calls for research support and private R&D contracts.

The ITACA Institute has eleven research groups of different sizes and two ungrouped researchers. At present time and according to the internal census, ITACA has more than one hundred people working on it.

The institute has an innovation manager and an administrative assistant. As they are little support staff for an institute of this size, some groups have incorporated their own innovation managers.

As a Spanish public university, the Universitat Politècnica de València depends on the regional government and the National Ministry with competencies in Universities.

3 Data and methods

We will measure the scientific production of the ITACA Institute and its components through the Annual Research Activity Index of a Research Structure (IAIE) and the Annual Research Evaluation Index (VAIE) [17], two indices that are calculated annually by the Universitat Politècnica de València based on the research and innovation merits recorded in its information systems. The Annual Research Activity Index of a Research Structure (IAIE) establishes a rating scale based on the amount and quality of various types of merits that have occurred during the year, mainly:

- Publication of results in research journals and research conferences.

– Competitive and collaborative funding achieved for research, development and innovation actions
– Positive evaluations of six-year research trams by the National Commission for the Evaluation of Research Activity (CNEAI).
– Direction and realization of doctoral thesis.
– Membership of congress committees and editorial committees of research journals.
– Patents and other intellectual property rights.

The Annual Research Evaluation Index (VAIE) tries to reduce the effect derived from the annual variability of the IAIE, taking into account the performance of the previous three years, having the most distant years less relevance:

$$VAIE(n) = IAIE(n) + \frac{3}{4}IAIE(n-1) + \frac{1}{2}IAIE(n-2) + \frac{1}{4}IAIE(n-3) \quad (1)$$

where $VAIE(n)$ is the VAIE index value for the year n, and $IAIE(n)$ is the IAIE index value for the year n.

These two indices are calculated at the end of the year after the one being evaluated. We will use provisional values of the indices for year 2018. As we are close to the end of the year, although the values could be given as almost definitive, there could be small differences with respect to the final values.

As staff census, we have used the Official Registry of Structures and Personnel of UPV (ROE Registry) [18]. We have chosen this registry, because UPV only estimates IAIE and VAIE for registered people.

The ROE Registry only includes personnel with work contracts lasting more than one year and who have formally requested their inclusion in it, with the exception of new full-time teaching personnel, who are assigned to their teaching department as ungrouped staff. We assume that personnel not included in the ROE Registry are not expected to have a relevant contribution to the scientific results of the structure.

The ROE Registry does not distinguish the different laboratories, groups or areas that exist in a research structure, so we use an internal census of ITACA Institute to associate researchers to the different research groups.

We also identify the personnel who has a PhD and is contracted full-time by the university. For that, we use the personnel categories of each person at the public directory of UPV.

Regarding the research groups, we associate a different number (from 1 to 9) to each group, excluding the groups that have two or less members, as we assume that they are more vulnerable to the annual variability of the scientific production indices. To reduce this effect, we are going to treat these very small groups as if they were one and associate them to number 10.

We define the VAIE of the group i in the year n as:

$$VAIE_i(n) = \sum_j VAIE_{ij}(n) \quad (2)$$

where $VAIE_{ij}()$ is the VAIE of the researcher j of the group i in the year n.

We define the VAIE of the research structure in the year n as the sum of the VAIEs of the different groups in the year n:

$$VAIE(n) = \sum_i VAIE_i(n) \tag{3}$$

We define the scientific contribution of the research group coded i to the research structure in the year n as:

$$SC_i(n) = \frac{VAIE_i(n)}{VAIE(n)} \tag{4}$$

We define the relation between registered members of the group i and registered members of the research structure in the year n as:

$$R_i(n) = \frac{M_i(n)}{M_T(n)} \tag{5}$$

where $M_i(n)$ is the number of members of the group i included at the ROE Registry and $M_T(n)$ is the number of registered members of the research structure. Of course, the following equation must be fulfilled:

$$M_T(n) = \sum_i M_i(n) \tag{6}$$

As a measure of the productivity of the groups we will analyze the scientific contribution of the groups in relation to their size. To do this, we define the scientific efficiency of a research group i in the year n as:

$$SE_i(n) = \frac{SC_i(n)}{R_i(n)} \tag{7}$$

Values greater than 1 indicate that the average contribution of the registered members in that group is higher than the average contribution of the registered members of the research structure. Values below 1 indicate that the average contribution of the members of that group is below the average contribution of a member of the research structure.

We define the relation between registered doctor members of the group i working full-time at UPV and registered doctor members of the research structure working full-time at UPV as:

$$Rp_i(n) = \frac{Mp_i(n)}{Mp_T(n)} \tag{8}$$

where $Mp_i(n)$ is the number of registered full-time doctor members of the group i included at the ROE Registry and $Mp_T(n)$ is the number of registered full-time doctor members of the research structure. Of course, the following equation must be fulfilled:

$$Mp_T(n) = \sum_i Mp_i(n) \tag{9}$$

We are also measuring the average scientific productivity of the full-time doctors of each group. For that, we define the scientific efficiency of the full-time doctors of a research group i in the year n as:

$$SEp_i(n) = \frac{SC_i(n)}{Rp_i(n)} \tag{10}$$

Instead of using the scientific contribution of a research group, we could define a scientific contribution of only the doctors of the research group, but the approach we are going to follow is that the VAIE of the research support staff is closely related to the scientific activities of the doctors of the group, so all the $VAIE_i(n)$ has been generated directly or indirectly by the full-time doctors of the group i.

Values greater than 1 indicate that the average contribution of the doctors in that group is higher than the average contribution of the doctors of the research structure. Values below 1 indicate that the average contribution of the doctors of that group is below the average contribution of a doctor of the research structure.

We are going to use the IAIE values to analize the profile of the different groups, according to the merits where they score more.

We define the IAIE of the group i in the year n as:

$$IAIE_i(n) = \sum_j IAIE_{ij}(n) \tag{11}$$

where $IAIE_{ij}(n)$ is the IAIE of the researcher j of the group i in the year n.

Table 1 provides descriptive statistics of registered members per group, registered full-time doctors per group, and IAIE and VAIE per group and per registered member.

Table 1. Descriptive statistics for the year 2018

	Minimum	Maximum	Average	St. Dev.
M_i	4	14	8.90	3.14
Mp_i	3	12	6.10	2.69
$IAIE_{ij}$	0	97.61	20.50	20.80
$IAIE_i$	71.23	327.50	182.43	74.95
$VAIE_{ij}$	0	284.06	49.03	55.43
$VAIE_i$	255.81	846.78	436.38	192.56

To analyze the research profile of each group, we analyze in detail its IAIE value and break it down into four categories (contracts and research projects, research journals and research conferences, positive evaluations of the six-year

research trams and other merits not included in the previous ones). From these values, we define four ratios that allow us to identify those types of merits in which each group has a greater deployment.

We define the ratio of IAIE of a research group associated to research contracts and projects in the year n as:

$$FUND_i(n) = \frac{\sum_j IAIEf_{ij}(n)}{IAIE_i(n)} \tag{12}$$

Where $IAIEf_{ij}(n)$ are the IAIE points of the member j of the group i associated to his/her performance in research contracts and projects in the year n.

We define the ratio of IAIE of a research group associated to publication of results in research journals and research conferences in the year n as:

$$ARTCi(n) = \frac{\sum_j IAIEa_{ij}(n)}{IAIE_i(n)} \tag{13}$$

where $IAIEa_{ij}(n)$ are the IAIE points of the member j of the group i associated to his/her performance in publishing results in research journals and research conferences in the year n.

We define the ratio of IAIE of a research group associated to the positive evaluations of six-year research trams by the National Commission for the Evaluation of Research Activity (CNEAI) in the year n as:

$$SXN_i(n) = \frac{\sum_j IAIEs_{ij}(n)}{IAIE_i(n)} \tag{14}$$

where $IAIEs_{ij}(n)$ are the IAIE points of the member j of the group i associated to his/her number of positive evaluations of six-year research trams by the National Commission for the Evaluation of Research Activity (CNEAI) in the year n.

We define the ratio of IAIE of a research group associated to other merits not included in the three previous ratios in the year n as:

$$OTHER_i(n) = \frac{\sum_j IAIEo_{ij}(n)}{IAIE_i(n)} \tag{15}$$

where $IAIEo_{ij}(n)$ are the IAIE points of the member j of the group i associated to other merits not included in the three previous ratios in the year n. Of course, the following condition must be fullfilled:

$$OTHER_i(n) = 1–(FUND_i(n) + ARTC_i(n) + SXN_i(n)) \tag{16}$$

Table 2 provides descriptive statistics of the merits ratios for the year 2018. The average values of these ratios allow us to know the general profile of the research structure. As expected for its orientation towards ICT applications, the most relevant scientific practices of ITACA Institute are those related to participation

Table 2. Descriptive statistics of merits ratios for the year 2018

	Minimum	Maximum	Average	St. Dev.
$FUND_i$	0.032	0.768	0.380	0.239
$ARTC_i$	0.100	0.497	0.270	0.147
SXN_i	0.030	0.435	0.227	0.157
$OTHER_i$	0.015	0.267	0.123	0.103

Table 3. Correlation coefficients for 2018 merits ratios

	$FUND_i$	$ARTC_i$	SXN_i	$OTHER_i$
$FUND_i$	1	-0.45	-0.52	-0.88
$ARTC_i$	-0.45	1	-0.48	0.35
SXN_i	-0.52	-0.48	1	0.36
$OTHER_i$	-0.88	0.35	0.36	1

in contracts and research projects. A correlation matrix for the 2018 merits ratios is presented in Table 3.

Regarding the analysis, the quantitative study will be complemented with information extracted from the members of the ITACA institute through informal interviews and other forms of information like the internal census of ITACA Institute.

4 Results

According to Tables 1 and 2, we can now conclude that the different ITACA groups have different sizes and profiles, taking into account the type of merits in which they concentrate their research activities.

The high inverse correlation between the ratio associated to research contracts and projects, and the ratio associated to other merits, detected in Table 3 is interpreted as researchers with intensive dedication to research projects and contracts do not find time, for example, to participate in editorial committees of scientific journals or to direct doctoral theses.

The different profiles of the research groups of ITACA Institute become even more noticeable in Table 4 and Figure 2, that presents the performance indicators of the groups in the year 2018.

The research group with the highest scientific efficiency is Group 3. However, it is a group that still has room for improvement since its production focuses on participation in research projects and contracts. Dedicating resources to the generation of scientific articles and participation in congresses, based on the results obtained in projects and contracts, would further improve their scientific production.

Table 4. Performance indicators of the ITACA groups in year 2018

	Mi	R_i	Mp_i	Rp_i	SC_i	SE_i	SEp_i	$FUND_i$	$ARTC_i$	SXN_i	$OTHER_i$
Group 1	14	0.16	4	0.07	0.13	0.79	1.91	0.28	0.50	0.03	0.19
Group 2	13	0.15	12	0.20	0.10	0.68	0.50	0.16	0.14	0.44	0.27
Group 3	10	0.11	4	0.07	0.19	1.73	2.96	0.77	0.12	0.07	0.04
Group 4	10	0.11	8	0.13	0.09	0.76	0.65	0.55	0.20	0.20	0.05
Group 5	10	0.11	8	0.13	0.07	0.60	0.51	0.07	0.26	0.44	0.24
Group 6	8	0.09	5	0.08	0.09	1.01	1.10	0.43	0.44	0.10	0.04
Group 7	8	0.09	7	0.11	0.15	1.67	1.31	0.03	0.47	0.24	0.26
Group 8	6	0.07	5	0.08	0.07	1.00	0.82	0.46	0.22	0.27	0.04
Group 9	4	0.04	3	0.05	0.06	1.30	1.19	0.57	0.26	0.08	0.08
Group 10	6	0.07	5	0.08	0.06	0.93	0.77	0.48	0.10	0.41	0.02

Fig. 2. ITACA groups performance in year 2018

Group 6 is the one that has a more balanced relationship between the projects and contracts in which they participate and the scientific articles they generate. The improvement measures should go towards the consolidation of some of the researchers as permanent staff.

Group 2 and Group 5 have very similar profiles. In fact, these two groups come from the division of the same group some years ago. The high weight of the positive evaluations of six-year research trams and the other merits in their profile indicates that they are mature groups. If we also take into account their scientific efficiency, we can conclude that they are groups whose leaders are close to retirement and who need to renew leadership, so measures to increase productivity should go in this direction.

Although it seems that Group 1 is more focused on scientific publications, the truth is that a good part of its funds come from innovation and educational projects that score lower in the IAIE. The good figure of the ratio related to research articles is due in part to the growing interest of the scientific community in a line of research in which they are pioneers. The low value of the indicator related to positive evaluations of six-year research trams indicates that improvement measures should go towards increasing the percentage of doctors working full time.

Group 4 is the one that has been part of the institute for less time. This is evident in the internal census, since the number of members almost doubles the number of registered people at the ROE Registry, becoming the largest group in personnel. As scientific publications usually come at the end of projects, it is expected that the ratio of research articles will increase in the coming years. The improvement measures should be aimed at the valorization of the projects results through scientific publications and the consolidation of the temporal staff.

The large difference between the ratios related to research projects and contracts, and scientific publications indicates that Group 7 is the closest to basic research. Improvement measures could be aimed at obtaining funds through public calls that finance excellent science.

Group 8 has some researchers who hold relevant positions in the university, which reduces the time they can devote to research. This is being noticed more in research articles than in the participation in research projects and contracts. The measures could be directed in this case to increase the research involvement of those researchers that do not hold relevant positions and the recruitment of PhD students.

Group 9 is another emerging group focused on participation in research projects and contracts and with good figures of scientific efficiency. In this case, improvement measures could be aimed at increasing the number of group members and the effort to disseminate the results of the projects through scientific articles.

Regarding Group 10, we can conclude that it is largely formed by senior researchers more focused on attracting funding through research projects and contracts than on scientific publications. Therefore, the potential measures could be aimed at facilitating the publication of scientific results. Although, since this

is the group in which we have included ungrouped researchers and two-member groups, a more exhaustive analysis would be necessary to obtain more appropriate measures.

5 Conclusions

We have shown that subsystems with different profiles coexist in a research structure. An analysis of these subsystems and their components facilitates the formulation of policies to increase the volume and quality of scientific production, specifically addressed to some of these subsystems.

We have also found that ITACA research groups that devote more time and effort to research projects and contracts, dedicate a low effort to participation in scientific committees of journals and conferences and to the direction of doctoral theses. However, extrapolating this statement to other research structures would require a broader and more exhaustive analysis than the one performed in this article.

It should also be taken into account that the work carried out has been a first approach to the systemic analysis of research structures, in which the influence of the external system has been taken into account in a very limited way (e.g., the number of positive evaluations of six-year research trams by the National Commission for the Evaluation of Research Activity of Spain).

We can take advantage of this systemic model by generating a formulation model by objectives [19] for each of the elements of the different levels (research structure, research groups and researchers). These formulation models could be based on a SWOT (strengths, weaknesses, opportunities and threats) analysis and a harmonization of the objectives of the different levels (systems, subsystems and components), so that the whole system works in the same direction. These models should be reviewed periodically to correct deviations in the execution, forming a PDCA (Plan-Do-Check-Act) cycle [20].

Acknowledgement

We thank the support given by the Research & Innovation Office of the Universitat Politècnica de València. We also thank the ITACA Institute members for their collaboration.

References

[1] Ferretti, F., Guimarães Pereira, A., Vértesy, A., Hardeman, S.: Research excellence indicators: time to reimagine the 'making of'? Science and Public Policy 45 (5), 731–741 (2018)

[2] Vertesy, D.: The Adjusted Research Excellence Index 2018: Methodology Report. Publications Office of the European Union (2019)

[3] Merigó, J. M., Cancino, C.A., Coronado, F., Urbano, D.: Academic research in innovation: a country analysis. Scientometrics 108 (2), 559–593 (2016)

[4] REF: REF 2019 Guidance on submissions (2019/01). Available at: https://www.ref.ac.uk/media/1092/ref-2019_01-guidance-on-submissions.pdf. (2019)
[5] Australian Research Council: ERA 2018 Evaluation handbook. Available at: https://www.arc.gov.au/file/10668/download?token=V5AKd-29. (2019)
[6] Tijssen, R.J.W.: Scoreboards of Research Excellence. Research Evaluation 12 (2), 91–103 (2003)
[7] Vitanov, N.K.: Science dynamics and research production. Springer International Publishing (2016)
[8] Australian Research Council: Linkage Program - ARC Centres of Excellence commencing 2020. Available at: https://www.grants.gov.au/?event=public.FO.showFOUUID=0AF2A4EB-EB83-18EA-118AFFE227395D92&keyword=CoE2020. (2018)
[9] Centres of Excellence in Research. https://www.aka.fi/en/research-and-science-policy/centres-of-excellence/ (date unknown, accessed 2019 Jun)
[10] What is a Center of Excellence. https://dg.dk/en/what-is-a-center-of-excellence/ (date unknown, accessed 2019 Jun)
[11] Ministerio de Ciencia, Innovación y Universidades: Orden CNU/320/2019, de 13 de marzo, por la que se aprueban las bases reguladoras para la concesión de ayudas públicas en el marco del Programa Estatal de Generación de Conocimiento y Fortalecimiento Científico y Tecnológico del Sistema de I+D+i y en el marco del Programa Estatal de I+D+i Orientada a los Retos de la Sociedad, del Plan Estatal de Investigación Científica y Técnica y de Innovación 2017-2020, destinadas a organismos de investigación y de difusión de conocimientos. BOE 69, 29527–29570 (21 March 2019)
[12] Cruz-Castro, L., Sanz-Menéndez, L.: The effects of the economic crisis on public research: Spanish budgetary policies and research organizations. Technological Forecasting and Social Change 113 (B), 157–167 (2016)
[13] von Bertalanffy, L.: General System Theory: Foundations, Development, Applications. George Braziller, New York (1968)
[14] Jackson, M.: Systems Approaches to Management. Springer US (2000)
[15] Dictionary.com: "excellent" definition. https://www.dictionary.com/browse/excellent. Rock Holdings Inc. (date unknown, accessed 2019 Jun)
[16] Hervás-Oliver, J.L., Boronat-Moll, C., Messana-Salinas, I.: Emprender en la Universidad Española: el caso de la Universidad Politécnica de Valencia. Economía Industrial 44, 115–123 (2017)
[17] UPV: Reglamento para la evaluación de la actividad de investigación, desarrollo, innovación y transferencia en la Universitat Politècnica de València. BOUPV 108, 99–153 (2017)
[18] UPV: Reglamento para las estructuras de investigación, desarrollo e innovación en la Universitat Politècnica de València. BOUPV 100, 52–94 (2016)
[19] Hernandis-Ortuño, B., Agustín-Fonfría, M.A., Esnal-Angulo, I.: Modelo sistémico para la gestión de empresas. Bernabé Hernandis Ortuño, Valencia (2017)
[20] Basu, R.: Implementing Quality – A Practical Guide to Tools and Techniques Thomson Learning, London (2004)

The ITACA-WIICT'18 is a meeting forum for scientifics, technicians and other professionals who are dedicated to Information and communication technologies study and research. Its fundamental scope is to promote the contact among scientific and professionals, improving the cooperation as well as the technological transfer among professionals.

Institute ITACA
Information and Communication Technologies

978-84-09-07373-3